

Combinatorial diversity of Syk recruitment driven by its multivalent engagement with FcεR1γ

Timothy Travers^{a,b,†}, William K. Kanagy^{c,d}, Rachael A. Mansbach^a, Elton Jhamba^{c,d}, Cedric Cleyrat^{c,d,‡}, Byron Goldstein^a, Diane S. Lidke^{c,d}, Bridget S. Wilson^{c,d}, and S. Gnanakaran^{a,*}

^aTheoretical Biology and Biophysics Group and ^bCenter for Nonlinear Studies, Los Alamos National Laboratory, Los Alamos, NM 87545; ^cDepartment of Pathology and ^dComprehensive Cancer Center, University of New Mexico, Albuquerque, NM 87131

ABSTRACT Syk/Zap70 family kinases are essential for signaling via multichain immune-recognition receptors such as tetrameric ($\alpha\beta\gamma\delta$) FcεRI. Syk activation is generally attributed to *cis* binding of its tandem SH2 domains to dual phosphotyrosines within FcεR1γ-ITAMs (immunoreceptor tyrosine-based activation motifs). However, the mechanistic details of Syk docking on γ homodimers are unresolved. Here, we estimate that multivalent interactions for WT Syk improve *cis*-oriented binding by three orders of magnitude. We applied molecular dynamics (MD), hybrid MD/worm-like chain polymer modeling, and live cell imaging to evaluate relative binding and signaling output for all possible *cis* and *trans* Syk–FcεR1γ configurations. Syk binding is likely modulated during signaling by autophosphorylation on Y130 in interdomain A, since a Y130E phosphomimetic form of Syk is predicted to lead to reduced helicity of interdomain A and alter Syk's bias for *cis* binding. Experiments in reconstituted γ-KO cells, whose γ subunits are linked by disulfide bonds, as well as in cells expressing monomeric ITAM or hemiITAM γ-chimeras, support model predictions that short distances between γ ITAM pairs are required for *trans* docking. We propose that the full range of docking configurations improves signaling efficiency by expanding the combinatorial possibilities for Syk recruitment, particularly under conditions of incomplete ITAM phosphorylation.

Monitoring Editor

Leah Edelstein-Keshet
University of British Columbia

Received: Nov 16, 2018

Revised: May 17, 2019

Accepted: Jun 10, 2019

INTRODUCTION

Spleen tyrosine kinase (Syk) is essential for signaling by B-cell receptors (BCR), Fc receptors for immunoglobulin G (FcγR), and Fc receptors for immunoglobulin E (FcεRI), all of which are members of the multichain immunorecognition receptor (MIRRs) family (Johnson *et al.*, 1995; Tamir and Cambier, 1998). Syk activation by MIRRs switches on multiple pathways in mast cells and B cells (Geahlen,

2009; Mocsai *et al.*, 2010), including protein kinase C (PKC) signaling (Kawakami *et al.*, 2000), the PI3K-mediated Akt pathway (Jiang *et al.*, 2003), and transcriptional regulation via the MAPK cascade (Wan *et al.*, 1996). The coupling of Syk to MIRRs relies on a tandem pair of Src homology 2 (SH2) domains in the N-terminal region (Geahlen and Burg, 1994). Both SH2 domains adopt the canonical SH2 fold, comprising a β-sheet flanked by two α-helices (Kuriyan and Cowburn, 1993), and bind to short peptide motifs carrying phosphotyrosine (pTyr) residues (Pawson, 1995). The two SH2 domains are connected by a 45-residue linker referred to as interdomain A, which consists of three α-helices in a coiled-coil conformation leading to a Y-shaped structure for the N-terminal region (Fütterer *et al.*, 1998). The only other member of the Syk family of nonreceptor protein tyrosine kinases is Zap70, which is expressed in T-cells and natural killer cells (Chan *et al.*, 1992; Chu *et al.*, 1998; Wang *et al.*, 2010) and whose N-terminal region also adopts a Y-shaped structure (Hatada *et al.*, 1995). In addition to binding pTyr motifs via its tandem SH2 domains (Kihara and Siraganian, 1994), the N-terminal region of Syk/Zap70 is also involved in the autoinhibition of its kinase domain (KD) through residue–residue interactions between interdomain A and the C lobe of the KD (Deindl *et al.*, 2007; Yan *et al.*, 2013). Syk and

This article was published online ahead of print in MBoC in Press (<http://www.molbiolcell.org/cgi/doi/10.1091/mbc.E18-11-0722>) on June 19, 2019.

*Address correspondence to: S. Gnanakaran (gnana@lanl.gov).

Present addresses: [†]New Mexico Consortium and Pebble Labs, Los Alamos, NM 87544; [‡]Juno Pharmaceuticals, Seattle, WA 98109.

Abbreviations used: BCR, B-cell receptor; IgE, immunoglobulin E; ITAM, immunoreceptor tyrosine-based activation motif; KD, kinase domain; KO, knockout; MD, molecular dynamics; MIRR, multichain immunorecognition receptor; RBL, rat basophilic leukemia; REMD, replica-exchange molecular dynamics; SH2, Src homology 2; TCR, T-cell receptor; TT, Tac-Tac; WLC, worm-like chain; WT, wild type.

© 2019 Travers *et al.* This article is distributed by The American Society for Cell Biology under license from the author(s). Two months after publication it is available to the public under an Attribution–Noncommercial–Share Alike 3.0 Unported Creative Commons License (<http://creativecommons.org/licenses/by-nc-sa/3.0>).

“ASCB®,” “The American Society for Cell Biology®,” and “Molecular Biology of the Cell®” are registered trademarks of The American Society for Cell Biology.

Zap70 can be functionally homologous for TCR and BCR signaling (Kong *et al.*, 1995; Cheng *et al.*, 1997), although Zap70 is more dependent on Src-family kinases (e.g., Lck) for its catalytic activation than Syk (Iwashima *et al.*, 1994; Fasbender *et al.*, 2017).

A distinguishing feature of the MIRRs, which lack intrinsic kinase activity, is the presence of pTyr-containing immunoreceptor tyrosine-based activation motifs (ITAMs) within the cytoplasmic tails of signaling subunits (Reth, 1989; Cambier, 1995; Sigalov, 2005; Harwood and Batista, 2008; Rivera *et al.*, 2008; Smith-Garvin *et al.*, 2009). MIRRs typically incorporate multiple ITAMs, often in disulfide-linked pairs such as the γ homodimers (common to Fc γ RIII, Fc γ RI, Fc ϵ RI), ζ homodimers (TCR), and Ig α ,Ig β heterodimers (BCR) (Reth, 2001). We focus here on high-affinity Fc ϵ RI, which is activated when multivalent antigens cross-link IgE–Fc ϵ RI complexes for increased defense against pathogens, wound healing, and allergic responses (Siraganian, 2003; Molfetta *et al.*, 2007; MacGlashan, 2008; Mukai *et al.*, 2018). Fc ϵ RI is an $\alpha\beta\gamma_2$ oligomeric complex with 3 ITAMs: one in the β subunit and one each in the disulfide-linked γ chains (Blank *et al.*, 1989; Ra *et al.*, 1989). In most models of ITAM-based signaling, phosphorylation of both tyrosines in the same ITAM is assumed to be required for docking of Syk's tandem SH2 domains (Kihara and Siraganian, 1994; Shiue *et al.*, 1995; Faeder *et al.*, 2003). This *cis*-binding orientation is supported by crystal structures of Syk and Zap70 bound to a single dually tyrosine-phosphorylated peptide (Hatada *et al.*, 1995; Fütterer *et al.*, 1998). Mass spectrometry-based analysis of Fc ϵ RI γ found that phosphorylation of the N-terminal Tyr is more abundant than of the C-terminal Tyr (Yamashita *et al.*, 2008), suggesting that ITAM phosphorylation is often incomplete and could limit availability for *cis*-oriented binding. The common presence of disulfide-linked ITAM-bearing pairs in the MIRRs, as mentioned above, raises the important question: do Syk (and Zap-70) bypass the requirement for full ITAM phosphorylation by docking in *trans* to pTyr pairs on adjacent signaling subunits? If so, is this alternative docking orientation equally efficient for signal propagation? We address these questions here through both modeling and experimental approaches.

Given that Syk has two distinct SH2 domains, we consider the evidence that individual SH2 domains show selectivity when interacting with phosphopeptides from their biologically relevant protein-binding partners. Prior studies have shown that SH2 domains exhibit 50- to 1000-fold higher affinity to phosphopeptides derived from binding partners than to randomized phosphopeptide sequences (Panayotou *et al.*, 1993; Songyang *et al.*, 1993; Ladbury *et al.*, 1995). Binding is also enhanced by multivalent interactions (Ottinger *et al.*, 1998), which is relevant for Syk–Fc ϵ RI, since the Syk tandem SH2 domains are bivalent and there are four available binding sites in a fully phosphorylated Fc ϵ RI γ chain homodimer. Other examples of signaling proteins incorporating tandem SH2 domains include the protein tyrosine phosphatases PTPN6 (or SHP-1; Pei *et al.*, 1996) and PTPN11 (or SHP-2; Pluskey *et al.*, 1995), as well as phospholipase C- γ 1 (Ji *et al.*, 1999). Interestingly, the recruitment of proteins bearing only a single SH2 domain, such as the phosphatase INPP5D (SHIP-1), is thought to be favored by monophosphorylation of BCR ITAMs (O'Neill *et al.*, 2011; Getahun *et al.*, 2016). In the case of Syk, experimentally measured binding affinities indicate micromolar affinity of individual SH2 domains to Fc ϵ RI γ , while engagement of the tandem SH2 domains results in stronger binding by around three orders of magnitude (Chen *et al.*, 1996). However, the relationship between multivalent binding on Syk–Fc ϵ RI γ stoichiometry and signal initiation remains of keen interest.

The ability of tandem SH2 domains to enhance Syk-ITAM occupancy can be impacted by posttranslational modifications in

interdomain A. We specially focus on Syk recruitment after phosphorylation at Y130 in interdomain A (Keshvara *et al.*, 1998), since Y130E substitution in Syk resulted in a phosphomimetic recombinant protein with reduced binding of its tandem SH2 domains to phosphorylated ITAMs in coimmunoprecipitation studies (Keshvara *et al.*, 1997; Zhang *et al.*, 2008). This was initially attributed to the structural destabilization of interdomain A and the resulting partial decoupling of both SH2 domains by the phosphomimetic mutation (Zhang *et al.*, 2008; Feng and Post, 2016; Roy *et al.*, 2016). However, high-resolution imaging studies in Syk-deficient cells reconstituted with Syk Y130E recombinant protein revealed two interesting observations: 1) Syk recruitment to Fc ϵ RI aggregates is retained even for Y130E phosphomimetic, and 2) impaired downstream signaling correlates with an increased off-rate for Fc ϵ RI–Syk(Y130E) interactions (Schwartz *et al.*, 2017). These results motivate the current studies to understand how interdomain A phosphorylation influences the conformation, binding orientation, and residency time of Syk's dual SH2 domains on ITAMs.

In this work, we examine Syk–Fc ϵ RI binding modes using a combination of conventional and enhanced-sampling molecular dynamics (MD) simulations, as well as hybrid MD/polymer theory (Sethi *et al.*, 2011). We first developed an analytical model based on simple structural arguments to evaluate how multivalent interactions cause a three-orders of magnitude increase in binding compared with that in individual SH2 domains. Next, conventional MD simulations show that Y130E substitution leads to increased flexibility in the relative orientations of the two SH2 domains in Syk. Replica-exchange MD (REMD) simulations of interdomain A further show that the amount of helical structure in this linker region is reduced by Y130E, thereby impacting the distance between the tandem SH2 domains. We then show using a hybrid approach of MD simulations and worm-like chain (WLC) polymer models that the combination of higher inter-SH2 distance and increased flexibility in the Syk Y130E mutant reduces its binding affinity to Fc ϵ RI γ in a *cis* orientation. Interestingly, wild type (WT) and Y130E mutant Syk show comparable affinities to Fc ϵ RI γ in WLC models of *trans* binding.

We also present structural models and binding energy estimates for the multiple *trans* binding modes that are possible for binding of two WT Syk molecules (one pair of tandem SH2 domains each) to a dimer of phosphorylated Fc ϵ RI γ chains (one pair of pTyr motifs each). Simulations predict that Syk tandem SH2 domains can bind phosphorylated γ -dimers effectively in both *cis* and *trans* orientations, with the caveat that the ITAM pairs must be in close proximity to accommodate *trans* binding. Given that the extent of ITAM phosphorylation is expected to be highly variable based upon antigen dose, valency, and occupancy of receptors by Ag-specific IgE, we propose that the availability of multiple *trans* and *cis* modes enhances the signaling capacity of Fc ϵ RI aggregates. Predictions of the computational modeling were supported by experiments in γ -KO rat basophilic leukemia (RBL- γ KO) cells reconstituted with disulfide-linked γ subunits bearing either WT or mutant ITAM sequences. Experiments in cells expressing chimeric receptor monomers incorporating the γ cytoplasmic tail provide novel insights into the classes of immunoreceptors that bear a single ITAM (e.g., Fc γ RIIA; Nimmerjahn and Ravetch, 2008) or a hemITAM (e.g., CLEC-2 or Dectin-1; Bauer and Steinle, 2017).

RESULTS

Impact of multivalency on the *cis*-oriented binding of wild type Syk tandem SH2 domains to a single Fc ϵ RI γ chain

We first constructed a structure-based analytical model that describes how local concentration effects lead to an enhancement of

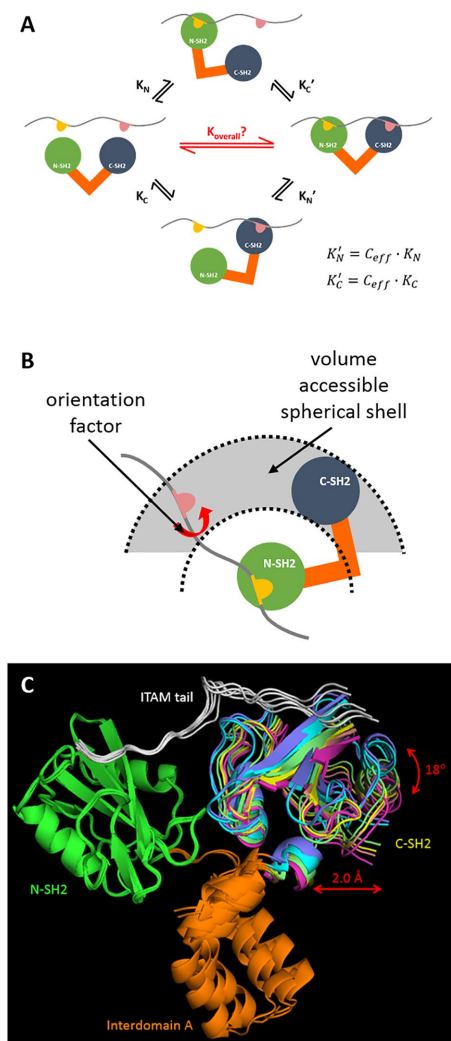


FIGURE 1: Structure-based analytical model for multivalent binding of Syk tandem SH2 domains to a single FcεR1γ chain. (A) Reaction network from unbound (left) to dual-bound (right) Syk. N-SH2, C-SH2, and interdomain A of Syk are shown in green, blue, and orange, respectively. The unstructured cytoplasmic region of the γ chain is shown as a wavy gray line, with pY64 and pY75 as pink and yellow symbols, respectively. (B) Schematic showing the accessible spherical shell where unbound SH2 can search for unbound ITAM and the orientation factor representing the flexibility of the γ chain, given prior binding of the other SH2:pTyr pair. Syk and the γ chain are colored as in A. (C) The six complexes in the asymmetric unit of the crystal structure of Syk tandem SH2 domains bound to CD3ε (PDB 1A81; Fütterer *et al.*, 1998) were structurally aligned at the N-terminal SH2 (green cartoons). The translational (2 Å) and orientational (18°) variability range for C-terminal SH2 (magenta to blue cartoons) among these six aligned complexes are shown with red arrows.

overall *cis* binding between the linked SH2 domains from Syk and the paired pTyr in a FcεR1γ chain ITAM. In Figure 1A, the initial binding steps of either N-SH2:C-ITAM or C-SH2:N-ITAM are shown with equilibrium association constants of K_N and K_C , respectively. The subsequent binding steps involve either 1) binding of C-SH2:N-ITAM after N-SH2:C-ITAM with an effective equilibrium association constant of K'_C , or 2) binding of N-SH2:C-ITAM after C-SH2:N-ITAM with an effective equilibrium association constant of K'_N . Both K'_N and K'_C are given by multiplying K_N and K_C by a factor C_{eff} that rep-

resents the effective concentration of unbound ITAM that unbound SH2 experiences upon binding of the other SH2:ITAM pair. This effective concentration factor is the same in both pathways described above (either binding of N-SH2:C-ITAM first or binding of C-SH2:N-ITAM first). This model is similar to the one we used previously to investigate the Grb2–Sos1 multivalent complex (Sethi *et al.*, 2011), where the effective equilibrium association constant for binding of both motifs, $K_{overall}$ (red arrows in Figure 1A), is given by

$$K_{overall} = C_{eff} \times K_N \times K_C \quad (1)$$

or the product of both monomeric association constants with the effective concentration.

To derive a relation for the effective concentration, we modeled the second binding step using the top path in Figure 1A, although the other direction will give the same results. The binding of the first SH2 domain restricts the region in space that the second SH2 domain can access. The effective concentration of sites the second domain can bind to is just the number of unbound pTyr in the accessible region that are oriented so that binding can occur, divided by the volume of the accessible region V_{acc} . We model V_{acc} as a spherical shell (colored gray in Figure 1B) with the bound SH2:ITAM pair at the center of the sphere. Based on the crystal structure of Syk tandem SH2 domains bound to CD3ε (PDB 1A81; Fütterer *et al.*, 1998) that contained six complex structures in the asymmetric unit cell, the spherical shell is located between 3.2 and 3.4 nm from the sphere center (C-SH2 translational variability of 2 Å in Figure 1C). The CD3ε chain also has an extended backbone in the crystal structure such that the inter-pTyr orientation can be assumed to be uniformly distributed between 0° and 360°; however, only a fraction of these orientations lead to successful complexes with Syk (C-SH2 orientational variability of 18° in Figure 1C). This can be expressed as an orientation factor (f_{or}) of 18°/360° or 0.05, which is the probability of the extended chain adopting an inter-ITAM orientation that allows multivalent binding with Syk. The effective concentration is thus given by

$$C_{eff} = \frac{1/N_A \text{ moles pYXXL}}{V_{acc}} \times f_{or} \quad (2)$$

where N_A is the Avogadro constant. We note that the binding orientation found in the crystal structure, where N-SH2 interacts with C-ITAM and C-SH2 with N-ITAM, is the only *cis* mode considered here. This is because a physical atomistic model cannot be built for the other *cis* mode, with interactions between N-SH2:N-ITAM and C-SH2:C-ITAM, since the linker sequence between the two ITAMs on a single γ chain is not long enough to accommodate these interactions (Supplemental Figure 1).

For the system shown in Figure 1C, the estimated C_{eff} is around 3.03 mM. The experimentally measured equilibrium dissociation constants for binding of doubly phosphorylated FcεR1γ tail to N-SH2 (K_N^D) and C-SH2 (K_C^D) are >2.3 and 1.3 μM (Chen *et al.*, 1996), respectively, whose reciprocals are K_N and K_C . Plugging these values into Eq. 1 and calculating the reciprocal of $K_{overall}$ gives an estimated value for the effective equilibrium dissociation constant ($K_{overall}^D$) of around 1 nM, which provides only a lower bound, since the value used for K_N^D is also only a lower bound. The experimentally measured value is 1.4 nM (Chen *et al.*, 1996). Thus, this simple analytical model captures the three-orders of magnitude multivalent effect observed in going from monovalent binding (with μM affinity) to bivalent binding (with nM affinity) between WT Syk tandem SH2 domains and the two pTyr in a single FcεR1γ chain.

Effect of the Y130E phosphomimetic mutation on Syk inter-SH2 distance

Our next goal was to use unbiased MD simulations to investigate the impact of interdomain A phosphorylation on the *cis* binding of Syk's tandem SH2 domains, using the Y130E phosphomimetic as a model system. The challenge of applying the earlier analytical model for the Syk Y130E mutant is that there is no experimentally resolved structure for this mutant. We thus turned to MD simulations to investigate how the Y130E mutation affects the structure of the tandem SH2 domains. We applied two order parameters to quantify the flexibility between SH2 domains in our simulations (Figure 2A). The first coordinate was the distance between C α 's of R21 on N-SH2 and R174 on C-SH2, which are both part of the pTyr-binding sites on their respective SH2 domains, and the second coordinate was the dihedral angle involving the C α 's of R21 and L28 on N-SH2 with R174 and V181 on C-SH2. These coordinates provided measures of inter-SH2 distance and orientation, respectively. For both constructs, seven simulation replicates were performed for 2 μ s simulation time per replicate.

These runs showed that the Y130E phosphomimetic has higher translational and orientational flexibility than WT Syk (Figure 2, B and C). We then chose two replicates per construct and extended the simulation time to 6 μ s per replicate, and found the same higher flexibility trends for the mutant as compared with the WT (Supplemental Figure 2). The higher flexibility seen in the simulations of the WT construct (Figure 2B) compared with the crystal structure (Figure 1C) is likely because the latter had a bound dually phosphorylated ITAM tail that constrained the inter-SH2 flexibility. Closer inspection of these simulations showed that, in contrast with experimental findings, there was no destabilization of the helical structure of interdomain A in the Y130E phosphomimetic (Supplemental Figure 3). We instead observed changes in the number of domain–domain contacts for Syk due to Y130E, particularly a decreased number of contacts between N-SH2/C-SH2 and C-SH2/interdomain A, as well as an increased number of contacts between N-SH2/interdomain A (Supplemental Figure 4). Overall there was a net loss of domain–domain contacts in these simulations, which may account for the increased flexibility of the Y130E mutant. We note that verification of the structural destabilization of interdomain A is not accessible within the time scales of unbiased MD simulations considered here.

To address this point, we next used an enhanced sampling simulation technique called replica-exchange MD (REMD) that allows more efficient sampling of the conformational ensemble for the system under study (Sugita and Okamoto, 1999; Garcia and Sanbonmatsu, 2001). The REMD simulations were limited here to residues K115 to T159 that comprise interdomain A, since we were interested here on Y130E-induced conformational changes in this linker and not in the SH2 tandem domains. This simplification by removal of both SH2 domains also allows for a smaller system size to further speed up conformational sampling of the linker. For the WT and Y130E constructs, we ran 63 replicas each within the temperature range 275–475 K, with 1.2 μ s of simulation time per replica for a cumulative simulation time of 75.6 μ s. Analysis was performed for each construct cumulatively on the 15 replicas with temperatures less than 310 K.

We again counted the number of helical bonds as a measure of the stability of the helical structure of interdomain A for both constructs in these simulations. Overall, we found that the Y130E mutant showed more helical unfolding than the WT construct, with around five helical bonds lost for Y130E compared with around two helical bonds for WT by the end of the simulations (Figure 3A). For the three individual helices that comprise the interdomain A struc-

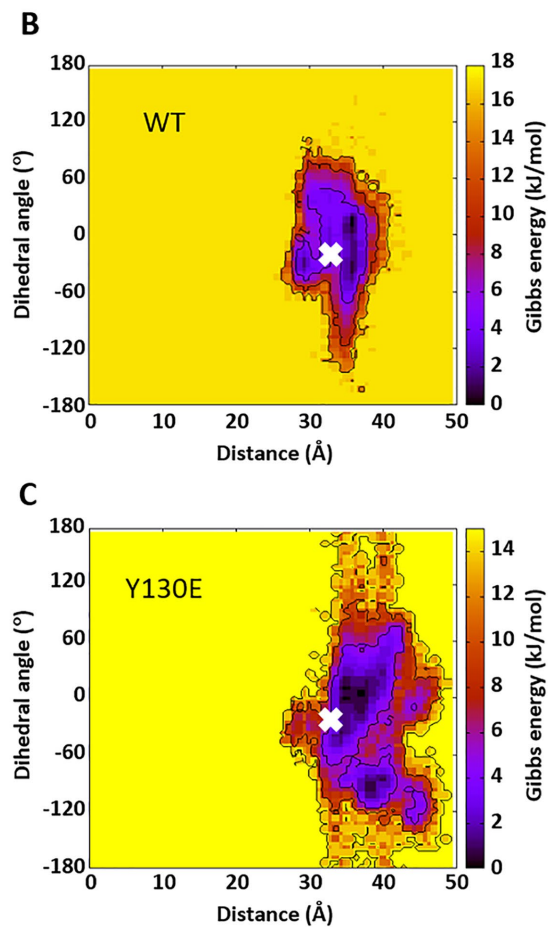
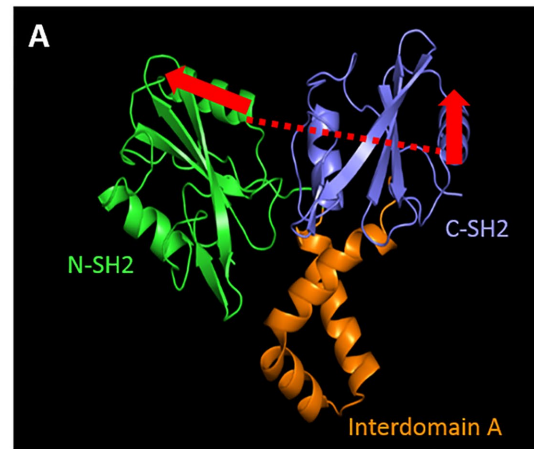


FIGURE 2: Unbiased MD simulations show higher inter-SH2 flexibility in the Y130E phosphomimetic form of Syk. (A) Distance (red dashed line) and dihedral (across red arrows) reaction coordinates for describing the inter-SH2 positions and orientations. (B) Free energy surface map for the WT Syk simulations based on the two reaction coordinates. (C) Corresponding free energy surface map for the Y130E phosphomimetic Syk. The white X in B and C gives the position of the starting conformation for the MD simulations. Data were collected from seven replicates per construct, with 2 μ s simulation time per replicate.

ture, we found that more unfolding occurred in helix 1 that contains the Y130 phosphorylation site, with the mutant destabilizing around three helical bonds in contrast to <1 for WT (Figure 3B). In contrast,

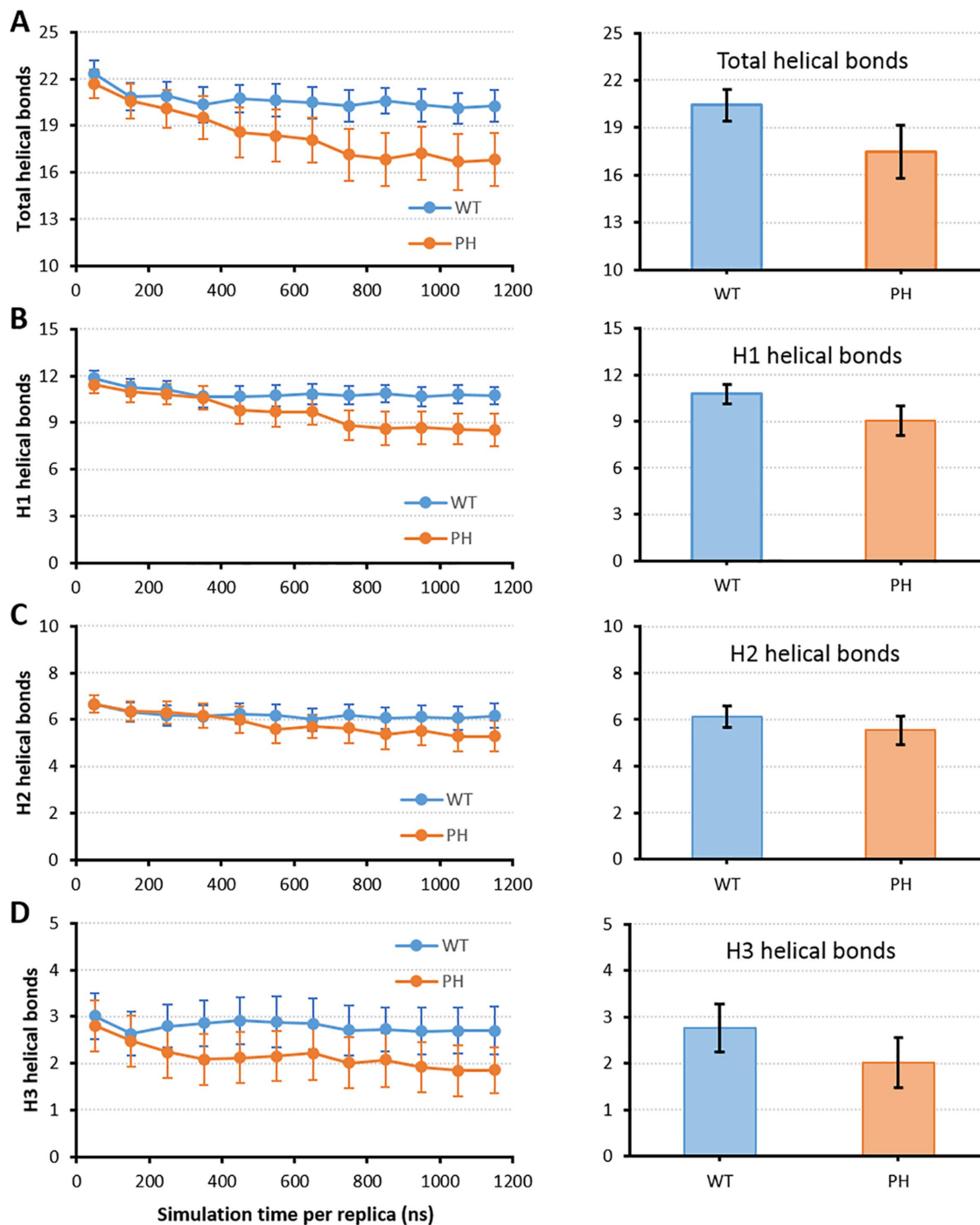


FIGURE 3: REMD simulations show more helical unfolding of interdomain A in the Y130E phosphomimetic mutant. Time profiles over the entire trajectory (left) and cumulative bar plots of the last 500 ns (right) for the number of helical bonds from REMD simulations of WT (blue) and Y130E mutant (orange) interdomain A. Helical bond counts were done for (A) total helices, (B) helix 1 (H1), (C) helix 2 (H2), or (D) helix 3 (H3). Error bars give SEM.

only around one helical bond was destabilized in helices 2 and 3 for the phosphomimetic mutant (Figure 3, C and D).

Given the helical unfolding observed here for Y130E, we were next interested to see how this might affect the distances between the SH2 domains. Thus, for the conformational ensembles obtained for the WT and Y130E interdomain A constructs in these REMD simulations, we reattached both SH2 domains in silico to every snapshot in order to assess the inter-SH2 distance distributions for both constructs. Given that the two ends of interdomain A were free

to move in the REMD simulations, we filtered for only those conformations that did not show steric clashes between N-SH2, C-SH2, and interdomain A upon reattachment of both SH2 domains. About 5% of the total number of models in both constructs remained physically viable after this filtering.

We found that the distance distributions for both constructs from the REMD-based models were broader than those from the unbiased simulations (Figure 4, A and B; compare with x axes in Figure 2, B and C), but consistently showed that the Y130E mutant

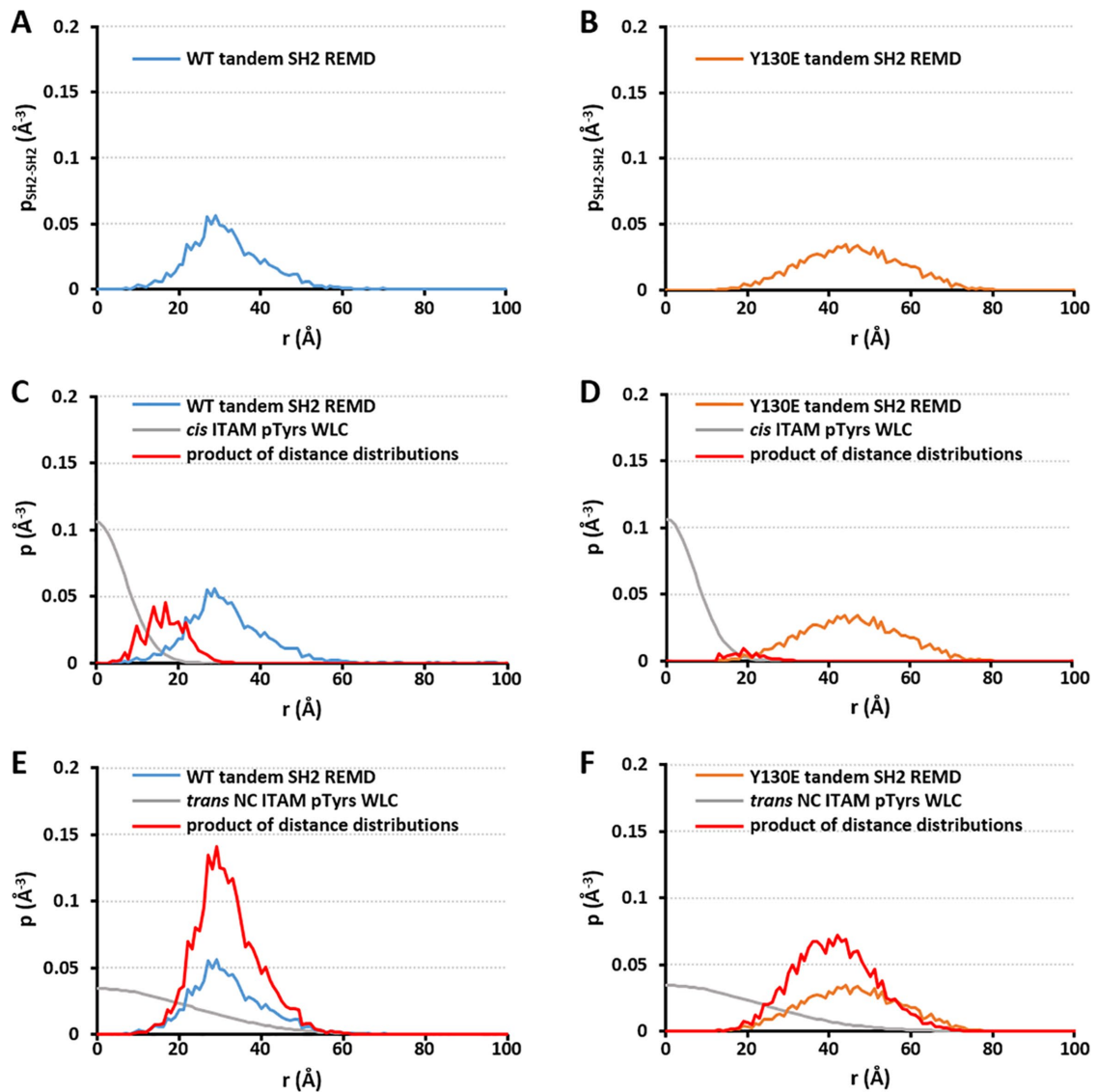


FIGURE 4: Distance distributions between tandem SH2 domains from REMD-based models and between ITAM pTyr from WLC models. (A) Distribution between SH2 domains from REMD-based models of WT tandem SH2. (B) Distribution between SH2 domains from REMD-based models of Y130E mutant tandem SH2. (C) The WT Syk distribution from A is shown with the distribution between ITAM pTyr from the WLC model of a single Fc ϵ R1 γ chain for *cis* binding (gray curve). (D) The Y130E Syk distribution from B is shown with the distribution between ITAM pTyr from the WLC model of a single Fc ϵ R1 γ chain for *cis* binding (gray curve). (E) The WT Syk distribution from A is shown with the distribution between ITAM pTyr from WLC model of two Fc ϵ R1 γ chains for *trans* binding (gray curve). (F) The Y130E Syk distribution from B is shown with the distribution between ITAM pTyr from WLC model of two Fc ϵ R1 γ chains for *trans* binding (gray curve). In C–F, the product of both distance distributions is shown by the red curve, whose integrated area gives C_{eff} . The magnitudes of the red curves have been increased here 100 \times to facilitate their visualization and comparison.

samples more inter-SH2 distance values than the WT. The mean inter-SH2 distance values for the WT construct were very similar, at around 32 Å, between the REMD-based models and the unbiased simulations. For the Y130E construct, however, the mean inter-SH2 distance was larger for the REMD-based models (around 46 Å) compared with the unbiased simulations (around 36 Å), which is consistent with the increased structural instability of interdomain A seen in the REMD simulations. Using these distance distributions, a hybrid MD/polymer approach can be employed to estimate the multivalent effect on binding for WT and Y130E mutant Syk to Fc ϵ R1.

Changes in multivalent *cis*-oriented binding of Syk to a single Fc ϵ R1 chain due to the Y130E mutation

As mentioned earlier, multivalent binding for Syk–Fc ϵ R1 depends on the effective concentration C_{eff} of unbound ITAM that unbound SH2 experiences when the other SH2:ITAM pair is bound. Given distance distributions between the Syk SH2 domains ($p_{\text{SH2-SH2}}$) and between the ITAM pTyr ($p_{\text{ITAM-ITAM}}$), it has been shown that C_{eff} can be calculated by determining the overlapping regions between the two distributions and integrating over the products of the probabilities in these regions for all possible distances (Van Valen *et al.*, 2009; Sethi *et al.*, 2011):

$$C_{\text{eff}} = \int_{r=0}^{\infty} p_{\text{SH2-SH2}}(r) p_{\text{ITAM-ITAM}}(r) d^3r \quad (3)$$

Here, we use the distance distributions derived from the REMD-based models of WT and Y130E mutant Syk tandem SH2 domains as the corresponding $p_{\text{SH2-SH2}}$ in Eq. 3. To derive $p_{\text{ITAM-ITAM}}$, we treat the FcεR1γ chains using a WLC polymer model. For binding of a Syk tandem SH2 to a single FcεR1γ chain (i.e., *cis* binding),

$$p_{\text{ITAM-ITAM}}(r; \text{cis}) = \left(\frac{3}{4\pi l_p l_c} \right)^{3/2} \times \exp\left(\frac{-3r^2}{4l_p l_c} \right) \quad (4)$$

where l_p and l_c are the persistence and contour lengths of the peptide between the two pTyr in the single FcεR1γ chain. Both of these length values can be expressed as a function of the number of residues in the peptide. The distance distribution plot for the *cis* binding WLC model is shown overlapped with corresponding plots for the WT and Y130E tandem SH2 REMD-based models in Figure 4, C and D. The C_{eff} values (proportional to the integrated area under red curves in Figure 4, C and D) for binding of a single FcεR1γ chain to WT and Y130E mutant Syk are estimated at 7.9 mM and 1.1 mM, respectively. These correspond to K_{overall}^D values of 0.38 and 2.8 nM, respectively, indicating that WT Syk has stronger affinity than the Y130E mutant for *cis* binding to a single FcεR1γ chain by around an order of magnitude. We note that the WT K_{overall}^D value calculated here using a hybrid MD/WLC model is close to that calculated earlier using an analytical model.

Trans-oriented multivalent binding modes increase the complexity of Syk recruitment toward FcεR1

The above hybrid MD/polymer model assumes that Syk only binds via a *cis* mode to an FcεR1γ monomer. However, an outstanding question is whether Syk can also span and bind to pTyr residues in both chains of an FcεR1γ dimer (i.e., *trans* binding). We first explored *trans* binding using a WLC polymer model to derive $p_{\text{ITAM-ITAM}}$ for the separate chains. For binding of a Syk tandem SH2 to separate pTyr on two FcεR1γ chains,

$$p_{\text{ITAM-ITAM}}(r; \text{trans}) = \left(\frac{3}{4\pi(l_p l_{c1} + l_p l_{c2})} \right)^{3/2} \times \exp\left(\frac{-3r^2}{4(l_p l_{c1} + l_p l_{c2})} \right) \quad (5)$$

where separate persistence and contour length values can be used for the two chains, based on the number of residues between the phosphotyrosine and the anchor point to the membrane surface (see Supplemental Appendix 1 for derivation). This distribution can then be used as input into Eq. 3, along with $p_{\text{SH2-SH2}}$ for Syk, to calculate C_{eff} . We note that there are three possible ways that *trans* binding of Syk to two FcεR1γ chains can occur: 1) binding to N-ITAM on one chain and to C-ITAM on the other chain (i.e., NC binding), 2) binding to N-ITAMs on both chains (i.e., NN binding), and 3) binding to C-ITAMs on both chains (i.e., CC binding).

The distance distribution plot for *trans* binding via the NC mode is shown overlapped with plots for the WT and Y130E tandem SH2 REMD-based models in Figure 4, E and F. The C_{eff} values for binding of WT and Y130E mutant to pTyr on separate construct chains are estimated at around 36.9 and 28.8 mM, respectively. These correspond to K_{overall}^D values of 0.08 and 0.10 nM, respectively, indicating that Y130E mutant Syk has affinity comparable to that of WT for *trans* NC binding. The corresponding distance distribution plots for *trans* binding via the NN and CC modes are shown in Supplemental Figure 5, and also show comparable affinities for WT and Y130E

mutants. For NN binding, the C_{eff} values for WT and Y130E mutants are 42.1 and 20.1 mM, respectively, leading to K_{overall}^D values of 0.07 and 0.15 nM, while for CC binding, the C_{eff} values for WT and Y130E mutants are 23.9 and 27.4 mM, respectively, leading to K_{overall}^D values of 0.12 and 0.11 nM.

We next applied computational modeling to explore how Syk molecules can bind to the ITAMs in the FcεR1γ dimer, using a maximum stoichiometry of two Syk molecules (a total of four SH2 domains) to one FcεR1γ dimer (a total of four pTyr). We assume here that all ITAM tyrosines have been phosphorylated. From a total of 24 possible permutations, we found that only six lead to viable atomistic models after structurally redundant or physically unrealistic models are filtered out. One of these six models is the *cis* binding mode, while the other five models are different *trans* binding modes (Figure 5A). Three of the five *trans* binding modes contain variations of *trans* NC binding (Trans1, Trans2, and Trans3 in Figure 5A), while the remaining two (Trans4 and Trans5) combine *trans* NN and *trans* CC binding.

Unbiased MD simulations for each of these 2:2 models of Syk–FcεR1γ were then performed using the soluble portions of the complexes, with three replicates per model at 1 μs simulation time per replicate. To evaluate the relative stability of each of these models, we used the linear interaction energy (LIE) method (Aqvist *et al.*, 1994) to compute the total free energies of the binding of ITAMs to their corresponding SH2 domains in each model. Results show that the *cis* orientation results in the highest binding free energy for WT Syk at a 2:2 stoichiometry between Syk–FcεR1γ (Figure 5B). Among the *trans* modes, Trans1 binding is strongest (80% of *cis*), followed by Trans4 (~70% of *cis*). Trans 2, 3, and 5 binding modes were feasible, but with interaction strengths approximately half that of *cis* binding.

We then assessed whether these differences in stability arise from interactions of individual Syk SH2 domains with the individual γ chain pTyr: the N-terminal pTyr site (pY64) or the C-terminal pTyr site (pY75). As shown in Supplemental Figure 6A, we computed interaction energies for each ITAM:SH2 pair and found similar results regardless of the binding mode. Two exceptions occur for pY75:N-SH2 in the Trans2 and pY64:N-SH2 binding in the Trans5 orientation; however these are due to unbinding of the pairs, which took place in only one out of three simulation replicates. Overall, the various binding modes do not appear to influence the affinity of individual Syk SH2 domains for particular ITAM pTyr strongly.

It is noteworthy that the interaction energies for binding of Syk's C-SH2 domain to pY64 in all orientations are predicted to be slightly higher than for the binding of the same C-SH2 domain to pY75 (Supplemental Figure 6B). Conversely, the binding of Syk's N-SH2 domain to pY75 is predicted to be slightly stronger than its binding to pY64. Supplemental Figure 6B also shows that, on average, Syk C-SH2 interactions with either pTyr site are stronger than the corresponding N-SH2 interactions. For most binding orientations, the simulations suggest that the interactions by Syk's N-SH2 domain are comparable. These results are qualitatively similar to experimental measurements of binding constants between individual Syk SH2 domains and CD3ε ITAMs, in the order pY64:C-SH2 > pY75:C-SH2 > pY75:N-SH2 > pY75:N-SH2 (Feng and Post, 2016).

We next considered the possibility that the engagement of tandem SH2 domains with both pTyr of the ITAM induces additional contact sites. As shown in Figure 6A, we made the novel observation that the interaction stability of a Syk tandem SH2 domain bound to a dually phosphorylated ITAM is improved by additional residue–residue interactions (red circles) of the C-SH2 domain with pY75 (which is bound to N-SH2). These interactions likely contribute to

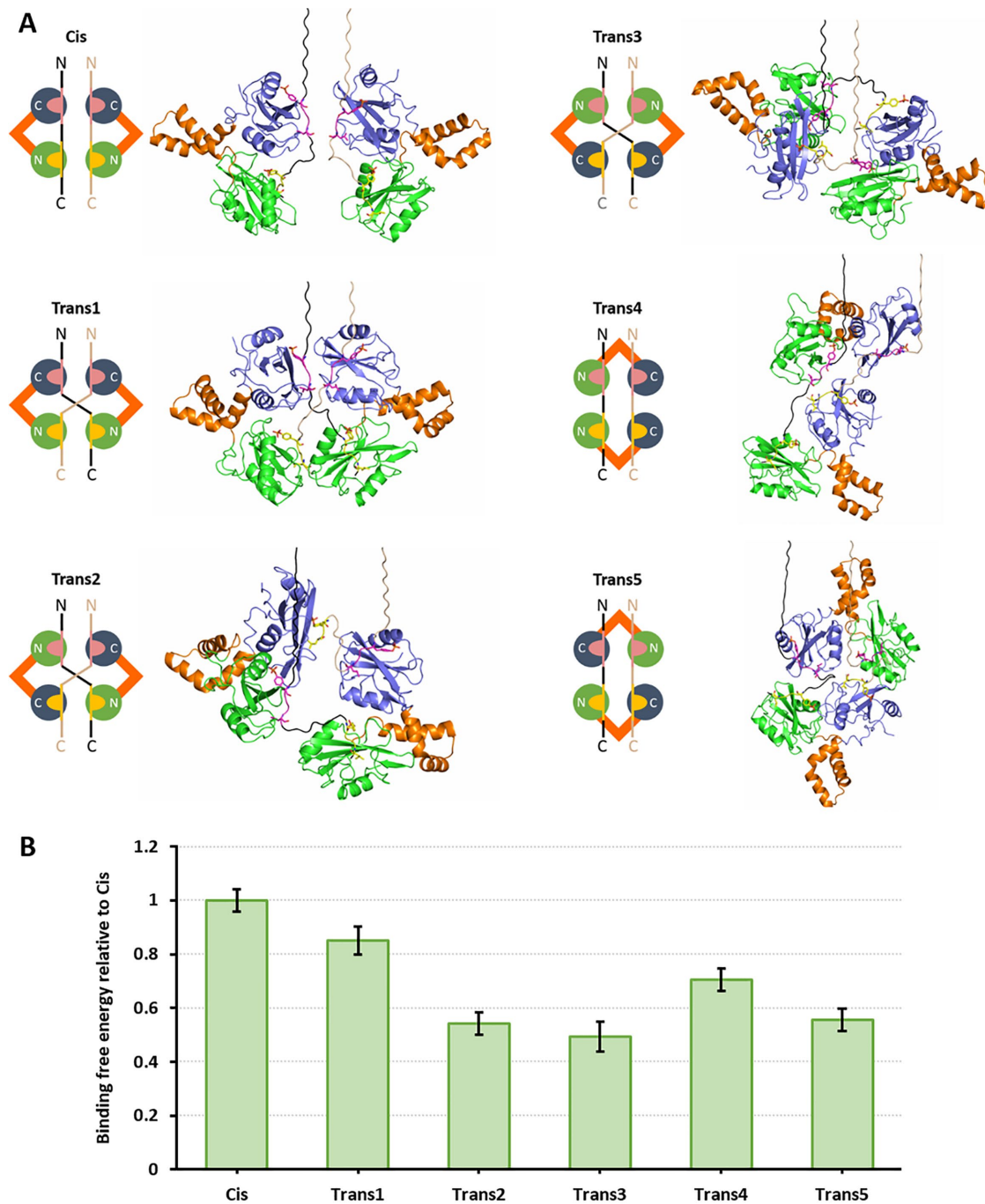


FIGURE 5: WT tandem SH2 domains show higher affinity for *cis* binding in complex models of Syk–FcεRI with 2:2 binding stoichiometry. (A) Diagrams and corresponding atomistic structures of one *cis* and five *trans* binding modes that are physically viable and consistent with a 2:2 binding stoichiometry. Syk is depicted here using cartoons for N-SH2 (green), C-SH2 (blue), and interdomain A (orange). In each model, the two γ chains are colored differently (black and light pink), and how pY64 (pink) and pY75 (yellow) are bound is shown. Portions of the linker that connect the N-terminal end of the ITAM to the γ -chain transmembrane helices are shown for each model using artificial extended conformations, to give a sense of how each model may be oriented relative to the surface of the cytoplasmic leaflet of the cell membrane. (B) Unbiased MD simulations of these models in solution were then performed, with the artificial linker regions that connect the ITAMs to the transmembrane helices removed. The overall binding free energies were then calculated using the linear interaction energy (LIE) method (Aqvist *et al.*, 1994) and are plotted here relative to the *cis* binding free energy. Error bars give SEM.

the stronger binding observed in *Cis* and *Trans1* orientations, as well as for *Trans4* (Figure 6B). Note that these unexpected contacts are asymmetric, as pY64 (which is bound to C-SH2) is not capable of additional interactions with N-SH2.

Figure 6C indicates that additional asymmetric contacts further contribute to the stability of Syk docking when engaged in 2:2 Syk–FcεRI γ complexes. The structural model shows that the pTyr and nearby residues of the γ chain bound to one Syk molecule are

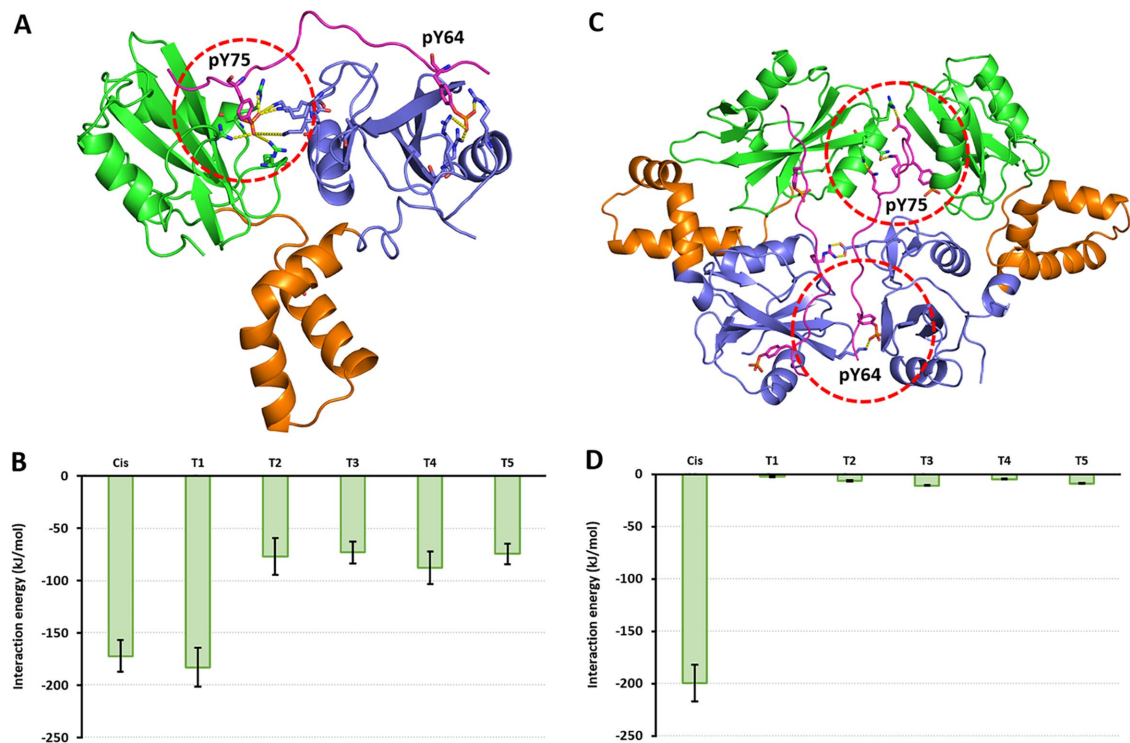


FIGURE 6: Additional contacts contribute to further stabilization of the *cis* binding mode. (A) Illustration showing that in the binding of the Syk N-SH2 domain to pY75 and the C-SH2 domain to pY64, asymmetrical contacts between pY75 and C-SH2 are formed (red circled region). This is not the case for pY64 and N-SH2. Key: N-SH2 (green), C-SH2 (blue), interdomain A (orange), γ chain (magenta). (B) Average interaction energies of these asymmetrical contacts when engaged in each of the different 2:2 binding modes. (C) Illustration of additional contacts between the pTyrS bound to the Syk molecule on the right with the “bystander” Syk molecule on the left (red circles) for the *cis* orientation of the 2:2 Syk–Fc ϵ R1 γ complex. Proteins are colored as in A. (D) Average interaction energies of these additional contacts, illustrating that these are significant only in the *cis* orientation. Error bars give SEM.

actually engaging in additional residue–residue contacts with the other Syk molecule (red circles). Because these interactions likely are unique to the *cis* orientation (Figure 6D), these data provide mechanistic support for the *cis* binding mode as the most stable mode of multivalent binding between Syk and Fc ϵ R1 γ (Figure 5B). We do note, however, that while individual *trans* modes are each weaker than the *cis* mode, the availability of multiple *trans* modes should allow a stronger gain for *trans* binding than for the single *cis* mode (see Figure 4, C and D for *cis* vs. E and F for *trans*).

Trans-oriented multivalent binding facilitates signaling during partial ITAM phosphorylation

We next evaluated experimentally the above computational predictions that formation of Syk–Fc ϵ R1 complexes can involve both *cis*- and *trans*-oriented binding modes. Experimental measures of calcium mobilization provide a sensitive indicator of Fc ϵ R1 and Syk activation in cultured mast cells (Smith *et al.*, 2001). We used two complementary approaches to study the Fc ϵ R1 γ ITAM–Syk axis in rat basophilic leukemia (RBL-2H3) cells. In the first approach, we took advantage of CRISPR-Cas 9 gene editing methods (Richardson *et al.*, 2016; Cleyrat *et al.*, 2017) to create RBL cells homozygous for the deletion of the ITAM-bearing γ subunit of Fc ϵ R1. Because complete assembly of the $\alpha\beta\gamma 2$ heterotetrameric complex is a prerequisite for trafficking of IgE receptors to the cell surface (Fiebiger *et al.*, 2005), we used cell sorting to select γ knockout cells based on a complete loss of binding to fluorescent IgE (unpublished data). This cell population was expanded in cell culture and then subjected to subcloning and Western blotting analysis to produce RBL cells com-

pletely lacking Fc ϵ R1 γ expression (Fc ϵ R1 γ -KO cells). This new cell line then served as the basis for Fc ϵ R1 reconstitution with γ constructs for expression of wild type gamma (γ WT) or mutants with substitutions of alanine for one or both tyrosine residues in the γ ITAM (γ Y64A; γ Y75A; γ Y64A\Y75A).

Results of this reconstitution model system to study Syk-dependent signaling are reported in Figure 7, based upon ratio imaging of cells loaded with the calcium reporter Fura-2AM (Smith *et al.*, 2001). Cells were primed overnight with Alexa⁶⁴⁷-IgE to screen for cells with comparable Fc ϵ R1 surface expression following transient transfection. As expected, antigen-mediated cross-linking of Fc ϵ R1 γ -KO cells reconstituted with γ WT led to marked elevation of cytoplasmic calcium in 100% of cells (Figure 7, A and B; Supplemental Figure 7, A and B). Prior work has shown that antigen stimulation of bone marrow–derived mast cells induces multiple species of Fc ϵ R1 γ phosphorylation (Yamashita *et al.*, 2008). If one assumes no bias for phosphorylation of the four tyrosines in the paired ITAMs, the resulting Fc ϵ R1 aggregates could represent up to 10 chemical species (four phosphorylation states per γ chain leading to 16 total states for two chains, although six of these states are redundant). This includes the full range from incompletely phosphorylated γ pairs (zero to three phosphotyrosines) to fully phosphorylated (four phosphotyrosines) that can recruit Syk in both *cis* and *trans* configurations, thereby increasing the combinatorial complexity of this system (Faeder *et al.*, 2005).

Cells reconstituted with γ Y64A or γ Y75A express Fc ϵ R1 complexes where each of the γ ITAMs can only be monophosphorylated. Thus, if Syk engages with two γ ITAMs through both of the

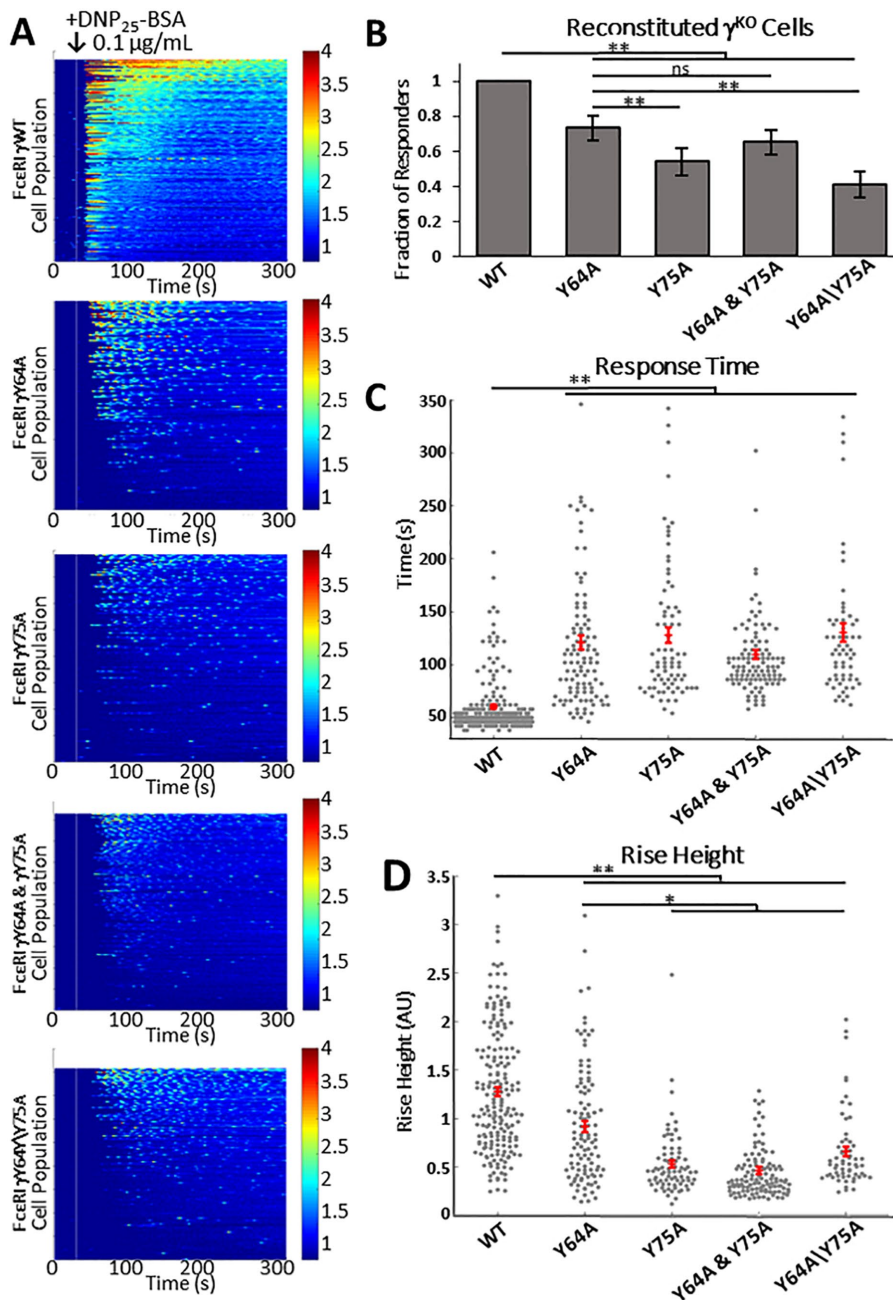


FIGURE 7: Calcium imaging of transiently FcεRIγ-reconstituted RBL-2H3 FcεRIγ-KO cells after antigen cross-linking supports the concept of *trans* docking of Syk onto pairs of monophosphorylated ITAMs, but with a greatly diminished response compared with that for *cis* docking. (A) RBL-2H3 FcεRIγ-KO were antigen cross-linked with DNP₂₅-BSA (0.1 μg/ml) calcium imaged after FcεRIγ reconstitution with (top to bottom) WT, Y64A, Y75A, a combination of Y64A and Y75A single mutants, or the double mutant Y64A/Y75A. (B) The respective percentages of response after antigen cross-linking. Error bars indicate the 95% CI. (C) The time between antigen cross-linking and calcium release. (D) The relative increase in the Fura-2 ratio per cell after antigen cross-linking. SEM and mean are reported in C and D by error bars and crosses, respectively. ** $P < 0.001$, * $P < 0.01$ by the Fisher test and the two-sample Kolmogorov–Smirnov test. Experiments were conducted over a period of 5 d.

SH2 domains in these cells, it can only be in one of the *trans* configurations. We observed the most consistent antigen-stimulated calcium responses in cells expressing γ subunits bearing only the ITAM Tyr75 residue (FcεRIγ-Y64A), where 73% of cells had a measur-

able change in cytosolic calcium (Figure 7, A and B; Supplemental Figure 7B). In comparison, calcium responses were triggered in only 54% of cells expressing γ subunits solely bearing ITAM Tyr64 (FcεRIγ-Y75A). Cells transiently transfected with both mutant γ constructs, which have the potential to express FcεRI composed of a mixture of γ Y75A and γ Y64A and could present a combination of all *trans* binding modes (see Figure 5A), showed calcium responses similar to those of cells expressing γ Y64A alone. Finally, cells reconstituted with the γ Y64A/ γ Y75A double mutant remain capable of triggering a weak calcium response, which may be attributed to the presence of an intact FcεRI β -ITAM.

Importantly, the profiles of calcium responses in cells that allow only two phosphorylation sites and a limited subset of *trans* binding modes were markedly less robust than in cells constituted with γ WT, where both *cis* and *trans* modes are possible in combination. Differences from γ WT include a slower onset for the initial calcium response (increase in response time, Figure 7C) as well as a lower overall magnitude of change (decrease in rise height, Figure 7D). They were also frequently highly oscillatory, which we classify as a weak response in Supplemental Figure 7C. The signaling output is weaker than in FcεRI aggregates reconstituted with γ WT, which also permit the full range of Syk binding configurations, including the canonical *cis* orientation as well as multiple *trans* orientations, depending on the extent of receptor phosphorylation.

Membrane anchoring distance is a critical factor in Syk recruitment in *trans*-oriented binding

We also explored the importance of proximity between ITAM pairs for recruitment of Syk in the *trans* binding mode, combining the power of experimental and modeling approaches. As an experimental strategy, we transiently transfected parental RBL-2H3 cells with plasmids encoding a chimeric Tac-Tac- γ (TT- γ) receptor monomer derived from the coding sequences of extracellular and transmembrane domains of the Tac antigen (IL2 α subunit) fused in frame with the γ subunit cytoplasmic tail sequence (Letourneur and Klausner, 1991; Wilson et al., 1995). We prepared vectors for expression of either WT chimeric receptors (TT- γ WT) or mutant versions with tyrosine-to-alanine substitutions in each of the two ITAM tyrosines (TT- γ Y64A, TT- γ Y75A and TT- γ Y64A/Y75A). The chimeric receptors are first converted to a quasidimer state by pretreating cells with Alexa⁶⁴⁷-tagged, murine monoclonal anti-Tac antibodies. Because this pretreatment does not initiate measurable mast cell signaling (Wilson et al., 1995), it provides a good model system to explore the role of distance in *trans* binding

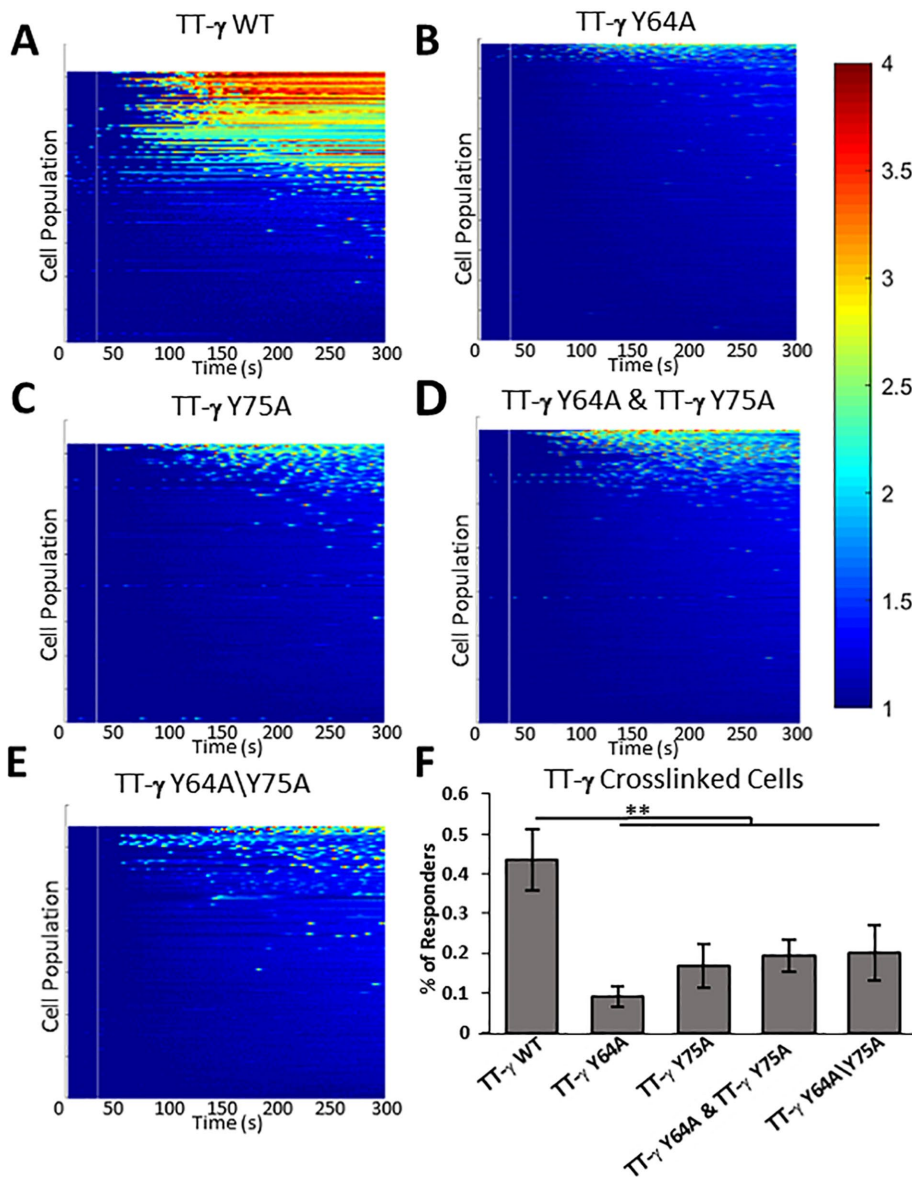


FIGURE 8: Calcium imaging after cross-linking of chimeric TT γ receptors demonstrates that Syk can bind *in cis* to a single ITAM but requires sufficiently close ITAMs for *trans* binding. Data are reported for RBL-2H3 cells transiently expressing (A) TT-Fc ϵ RI γ (WT), (B) TT-Fc ϵ RI γ (Y64A), (C) TT-Fc ϵ RI γ (Y75A), (D) the combination of TT-Fc ϵ RI γ (Y64A) and TT-Fc ϵ RI γ (Y75A), or (E) TT-Fc ϵ RI γ (Y64A\Y75A). Cells were preincubated for 10 min with Alexa⁶⁴⁷-labeled anti-Tac murine monoclonal antibodies and then cross-linked with anti-mouse secondary antibodies, as described in *Materials and Methods*. Heat maps indicate Ca²⁺ mobilization, with red indicating a strong response and blue indicating no release. (F) The respective percentages of response after TT cross-linking. Error bars indicate the 95% CI. ** $P < 0.001$ by the Fisher test. Experiments were conducted over a period of 5 d.

for Syk. We again used Alexa⁶⁴⁷ labeling as a thresholding method to select transiently transfected cells with comparable surface expression of chimeric receptors.

Results in Figure 8 show that aggregation of TT- γ WT chimeric receptors with anti-mouse secondary antibodies led to robust calcium responses in 41% of the cells examined, with weak and oscillatory calcium bursts in an additional 2% of cells (Figure 8, A and F; Supplemental Figure 7D). These data confirm that aggregation of receptor monomers with a single γ ITAM is generally less efficient at signaling than stimulation via cross-linking of the intact receptor

(see Figure 7). Weaker responses were observed after aggregation of either of the TT- γ mutant forms, where only monophosphorylation is possible (TT- γ Y64A and TT- γ Y75A; Figure 8, B and C). As summarized in Figure 8F and Supplemental Figure 7D, these responses were limited to a small fraction of cells examined and are not significantly better than for cells expressing TT- γ chimeras that lack both tyrosines (TT- γ Y64A\Y75A; Figure 8, E and F). Cotransfection of TT- γ Y64A and TT- γ Y75A into RBL-2H3 cells led to the possibility of mixed TT- γ aggregates containing both monophosphorylated forms of the γ ITAM but did not improve the consistency of responses after cross-linking (Figure 8, D and F). The inability of TT- γ single-tyrosine mutants to signal is consistent with the separation between cross-linked TT- γ outside the limits of the binding distance calculated for SH2 domains (Figure 4; Supplemental Figure 5).

DISCUSSION

Efficient immune-cell signaling relies on protein–protein interactions, which are often facilitated by reversible phosphorylation events (Hunter, 1995; Pawson and Scott, 2005; Basson, 2012; Ardito *et al.*, 2017; Gelsen *et al.*, 2018). The recruitment of the Syk/Zap-70 family of cytosolic tyrosine kinases to ITAM motifs is an essential step in signaling by the MIRR family of immunoreceptors (Geahlen, 2009; Mocsai *et al.*, 2010). In this work, we have applied multiple computational modeling approaches to characterize the structural features that control interactions between Syk and the Fc ϵ RI γ -ITAM. We report contributions of multiple factors to the specificity and strength of the Syk–Fc ϵ RI complex, including how the combination of multivalency and *cis* versus *trans* binding orientations increases signaling output in situations where phosphorylation of γ -ITAMs is incomplete. We unveil novel residue–residue interactions made possible only in specific orientations. We also provide mechanistic insight into the impaired binding of the Syk-Y130E that mimics structural changes induced by phosphorylation in interdomain A.

The influence of multivalency was explored through development of a structure-based analytical model (Figure 1). We show that local concentration effects arise due to the bivalent nature of Syk's tandem SH2 domains together with the paired pTyr in the Fc ϵ RI γ -ITAM. We applied an effective equilibrium association constant for binding of the linked motifs, previously derived (Sethi *et al.*, 2011), that comprises the product of the two monomeric association constants and a quantity called C_{eff} as shown in Eq. 1. C_{eff} represents the effective local concentration of pTyr available for SH2 binding, given that one SH2:pTyr is already engaged. We used

the translational variability between the Syk tandem SH2 domains observed in the six structures from PDB 1A81 (Fütterer *et al.*, 1998) to define the volume of the spherical shell where unbound SH2 can search for unbound pTyr. The orientational variability between the tandem SH2 domains in these six structures was also used to obtain a factor for the fraction of orientations within this search shell that allow for successful binding events. Combining these values with the experimentally measured monomeric binding constants (Chen *et al.*, 1996), we arrived at a calculated effective binding constant of ~1 nM for the system, which is consistent with the experimentally measured affinity for Syk SH2–SH2 bound to a dually phosphorylated ITAM (Chen *et al.*, 1996).

Binding characteristics of the Syk Y130E mutant are particularly of interest, since expression of this phosphomimetic has impaired signaling capability (Schwartz *et al.*, 2017). Because there is no resolved structure for the phosphomimetic, we used a hybrid MD/polymer model to generate two distance distributions (inter-SH2 for Syk and inter-pTyr for FcεR1γ). First, the inter-SH2 distance distribution was computed from unbiased MD simulations of the Syk tandem SH2 domains connected by the interdomain A linker using WT and Y130E mutant constructs. These simulations showed that the mutant sampling conformations cover a wider distance distribution than the WT (x-axes in Figure 2, B and C). The mutant also shows higher orientational variability in the conformations it sampled in these simulations (y-axes in Figure 2, B and C). These conformational differences were attributed to changes in the number of domain–domain contacts in the mutant relative to the WT construct (Supplemental Figure 4). In particular, there is a decrease in the number of contacts between the N-SH2 and C-SH2 domains in the presence of the mutation, which is consistent with the experimentally observed partial decoupling of both SH2 domains in the mutant (Zhang *et al.*, 2008; Feng and Post, 2016; Roy *et al.*, 2016).

MD simulations provided insufficient information on the influence of the Y130E substitution on helical stability, due to limited sampling even at microsecond time scales. Motivated by experimental observations that Y130E does disrupt helical stability (Zhang *et al.*, 2008; Feng and Post, 2016; Roy *et al.*, 2016), we computed inter-SH2 distance distribution from REMD simulations of the interdomain A linker. Only the linker was included in these simulations in order to enhance the sampling of adopted conformations and to evaluate the impact of the Y130E mutation. The two SH2 domains were then reattached to each conformation in the WT and Y130E interdomain A ensembles, from which the inter-SH2 distance distribution was obtained after filtering of models that showed large steric clashes when both SH2 domains were added back. The models based on the REMD simulations of Y130E linker showed more unfolding of helical turns than the WT model (Figure 3). The inter-SH2 distance distribution for Y130E in these simulations was broader and had a higher average value than WT (Figure 4, A and B).

A major uncertainty in these calculations is that the FcεR1γ cytoplasmic tail is structurally disordered; adequate conformational sampling of these unstructured regions is challenging for MD simulations (Lopez *et al.*, 2015) even using enhanced sampling techniques. To evaluate the inter-pTyr distance distribution within an ITAM, we used a WLC polymer model. When applied to protein chains, WLC modeling derives this distance distribution (gray curves in Figure 4, C and D) based on Eq. 4 as a function of the persistence and contour lengths. These length values provide the minimum length where the polymer can be modeled as a random walk and the maximum possible length of the polymer, respectively (Zhou, 2001; Ohashi *et al.*, 2007; Rawat and Biswas, 2009). The product of the two distributions at each distance value is shown as a red curve in Figure 4, C and D,

and integrating the area under this curve gives an estimate of C_{eff} as given in Eq. 3. The effective binding constant for the Y130E Syk mutant was found to be ~10-fold lower than that for the WT. Taken together, these data support the experimental observation that the Y130E phosphomimetic form of Syk can be recruited to FcεR1 complexes. If the 10-fold lower binding is mainly attributable to an increased k_{off} (i.e., higher dissociation rate of formed complexes), then this would be consistent with the experimentally observed shorter lifetimes of bound Y130E mutant Syk (Schwartz *et al.*, 2017).

Many MIRRs incorporate paired ITAM-bearing subunits, including the FcεR1γ₂ subunit (shared with Fcγ receptors), as well as TCRζ₂ and the BCR Igα–Igβ complex. These paired homodimers and heterodimers are stable by virtue of a disulfide linkage (Turner and Kinet, 1999; Call *et al.*, 2006). This markedly expands the complexity and number of variations for possible multivalent interactions, in comparison to the simplest case considered in Figure 1 for Syk tandem SH2 domains bound to paired pTyrs in the *cis* orientation. We used WLC polymer models along with molecular modeling and simulations to explore the possibility that Syk can also bind stably to γ homodimers via several *trans* orientations. WLC polymer models for native FcεR1γ chains showed that *trans* binding can be comparable to or stronger than *cis* binding (see Figure 4, C and D for *cis* vs. E and F for *trans*). Even in the cases where individual *trans* modes are less efficient than the *cis* configuration for recruiting Syk (Figures 5 and 6), the availability of multiple *trans* modes vs. a single *cis* mode should allow enhanced opportunities to recruit Syk, given the evidence that multiple phosphorylation states are generated following receptor activation (Yamashita *et al.*, 2008).

We tested predictions of the model by performing experiments in FcεR1γ-KO cells, where the intact receptor is reconstituted with either WT or Tyr-mutant versions of the γ cytoplasmic tail (Y64A and Y75A). Signaling is maximal in cells reconstituted with the WT form, which offer a full range of *cis* and *trans* docking modes in response to multivalent antigen (Figure 7, A and B). Receptors bearing mutant γ constructs are composed of disulfide-bonded γ homodimers with two, rather than four, ITAM tyrosines. Importantly, aggregation of these homodimers can generate measurable calcium responses when only *trans* binding modes are available for docking a single dual SH2 domain of Syk, but with markedly less robust responses (Figure 7, B–D). Our results are consistent with previous studies where γ-ITAM tyrosine mutants were expressed in γ-knockout bone marrow-derived mast cells (Yamashita *et al.*, 2008), which focused on potential dephosphorylation kinetics rather than Syk orientation as a mechanism for controlling signal propagation. In addition, we point out that the β-ITAM is intact in the FcεR1γ reconstituted receptor complexes, and therefore we cannot rule out it contributing in part to Syk recruitment in the intact receptor. Indeed, this is supported by the observation that weak calcium signaling was observed on antigen stimulation of FcεR1γ KO cells after reconstitution with γ constructs deficient in both Tyr75 and Tyr64 (γY64A\Y75A).

We also compared signaling capabilities in cells expressing chimeric receptor monomers, where the transmembrane and extracellular domains of the Tac antigen (IL2α subunit) is fused to the γ cytoplasmic tail. We confirmed that extensive cross-linking of the WT version of the TT-γ receptor leads to a robust calcium response (Figure 8), although the response rate is less consistent than for cells with WT FcεR1γ reconstituted receptor complexes. These results are consistent with the distances of antibody–cross linked WT TT-γ constructs, which likely favors a *cis* orientation for Syk binding. We speculate that this behavior is relevant to signal initiation by monomeric receptors containing a single functional ITAM, such as FcγRIIA (Van den Herik-Oudijk *et al.*, 1995).

We also generated chimeric TT- γ receptors with alanine substitutions at Y64 or Y75 that are similar to the naturally occurring class of "hemITAM" receptors, which include CLEC-2 and Dectin-1 (Bauer and Steinle, 2017). Because each monomer has a single tyrosine phosphorylation site, they can recruit Syk only via *trans* binding modes. Distance is again a contributing factor. We hypothesize that the very weak signaling observed for these mutant chimeric constructs is due in part to the limits of the experimental system, where dimerization with anti-Tac antibodies separates the two chains by a wide distance. We note that based upon a Fab separation distance of ~ 120 Å in a typical IgG antibody (Harris *et al.*, 1998), we expect that *trans* binding is essentially precluded, because the WT and Y130E mutant inter-SH2 distributions cover shorter distances (<80 Å; see Figure 4, A and B), leading to almost no overlap between the distributions and thus very small values for C_{eff} .

On the surface, the relative signaling capabilities of *cis* and *trans* configurations for Syk docking are distinguishing features that strikingly separate several distinct classes of immunoreceptors bearing either ITAM or hemITAM domains. Modeling predictions support the notion that multisubunit receptors that take advantage of multiple orientations for Syk docking should be the most efficient for signal transduction. We expect that this principle also applies to receptors that couple to other tandem SH2 domain-containing proteins, such as Zap-70, PTPN6, PTPN11, and PLC- γ 1 (Pluskey *et al.*, 1995; Pei *et al.*, 1996; Ji *et al.*, 1999). However, there are still lessons to be learned about the recruitment of Syk to ITAM receptors under conditions of suboptimal cross-linking, where monophosphorylation of ITAMs is expected to predominate (O'Neill *et al.*, 2011; Mahajan *et al.*, 2014). In the case of hemITAM receptors, which have only one tyrosine phosphorylation site per monomer, these are limited to a *trans* binding mode for Syk recruitment. We speculate that the membrane anchor distance between hemITAMs after aggregation of this entire class of C-type lectin-like receptors will be the key determinant of signaling output, where *trans* docking must be the key event after dimerization (Hughes *et al.*, 2010). In particular, a geometrical approach for quantifying multivalency when both chains are separated by a distance d between their membrane anchor points (see Supplemental Appendix 2 for derivation) indicates that C_{eff} , and thus the multivalent binding affinity of Syk, is inversely proportional to the square of distance d . This suggests a possible mechanism where the cell can modulate the binding of Syk to hemITAMs via changes in gene expression that can regulate the membrane density, and thus membrane spacing, between hemITAMs. A relatively weak signaling capability for Dectin-1 may also explain the need for a high density of surface-exposed β -1,3-Glucan on pathogens to trigger phagocytic responses to yeast (Wester *et al.*, 2017; Graus *et al.*, 2018).

MATERIALS AND METHODS

Analytical model of multivalent interactions in WT Syk-Fc ϵ R1 γ complex

The crystal structure of the Syk tandem SH2 domains bound to the ITAMs from a single CD3 ϵ tail (PDB 1A81; Fütterer *et al.*, 1998) was used here to quantify the possible changes in Syk upon its binding to an immunoreceptor. In particular, the six complexes in the asymmetric unit cell of this crystal structure were compared after structural alignment of their N-SH2 in PyMOL (Schrödinger), which showed that the C-SH2 position varied within a range of 2.0 nm (i.e., translational variability) and the C-SH2 rotation varied within a range of 18° (i.e., orientational variability). The translational and orientational variabilities were used to compute the V_{acc} (volume of accessible spherical shell) and f_{or} (orientation factor) terms in Eq. 2, which

gives the effective concentration C_{eff} of unbound ITAM that unbound SH2 experiences upon binding of the other SH2:ITAM pair. This effective concentration can then be used in Eq. 1 to estimate the effective equilibrium association constant K_{overall} for multivalent Syk-Fc ϵ R1 γ , whose reciprocal is the effective equilibrium dissociation constant $K_{\text{overall}}^{\text{D}}$, which can be compared with experimental measurements.

System setup and unbiased MD simulations of Syk tandem SH2 and interdomain A

Chain A from PDB 1A81 was used as the initial conformation for performing unbiased MD simulations of Syk tandem SH2 and interdomain A. This chain contains the WT human sequence, and in silico mutagenesis was done using PyMOL to generate the WT murine sequence comprising residues 8–261. The initial conformation for the Syk Y130E mutant used this WT construct with the single phosphomimetic mutation done in silico using PyMOL. Acetyl and N-methyl neutral caps were added to the N- and C-termini of both constructs using PyMOL. All-atom topologies and parameters for both constructs were generated using the CHARMM36 force field (Klauda *et al.*, 2010; Best *et al.*, 2012). Solvent molecules were added using the TIP3P water model (Jorgensen *et al.*, 1983) to fill a rhombic dodecahedral box around each construct, with a minimum distance of 1.2 nm from any protein atom to any edge of the simulation unit cell. Monovalent K⁺ and Cl⁻ ions were added to neutralize the system charge and to reach a physiological ionic strength of 150 mM.

The AMBER MD engine (version 16), which has been GPU-optimized for simulating explicit solvent systems (Salomon-Ferrer *et al.*, 2012; Case *et al.*, 2017) was used for running unbiased MD simulations of the Syk WT and Y130E systems. Particle mesh Ewald (PME) electrostatics (Darden *et al.*, 1993) was used along with Coulomb and Lennard Jones cutoffs of 1.2 nm and potential switching at 1.0 nm. A constant temperature was maintained at 310 K via Langevin dynamics (Pastor *et al.*, 1988) with a collision frequency of 1.0 ps⁻¹. Semiisotropic pressure coupling was set for each system at 1 bar using a Monte Carlo barostat (Åqvist *et al.*, 2004) with a relaxation time of 4.0 ps. Bonds containing hydrogen atoms were constrained using the SHAKE algorithm (Ryckaert *et al.*, 1977). A hydrogen mass-repartitioning approach (Feenstra *et al.*, 1999) allowed the use of a 4-fs time step. Both systems were energy-minimized using up to 10,000 steps of steepest descent. Seven replicates of each system were then equilibrated, with each replicate having different initial velocities. Position restraints were applied to all protein heavy atoms during equilibration, which took 100 ps in the NVT ensemble and 10 ns in the NPT ensemble. Production runs (without position restraints) of 2 μ s in the NPT ensemble were then performed for each replicate with configurations and energies saved every 200 ps. Two out of seven replicates were randomly selected for each system, and the simulations extended to 6 μ s. Analyses were performed on the last two-thirds of each simulation. The distance reaction coordinate was measured between the C α atoms of residues R21 and R174, which are part of the corresponding pTyr-binding sites on N-SH2 and C-SH2, respectively. The dihedral reaction coordinate was measured using the C α atoms of R21 and L28 from N-SH2 with R174 and V181 from C-SH2, which belong to stable α -helices near the pTyr-binding site of each SH2 domain.

System setup and REMD simulations of Syk interdomain A

The initial conformation for performing REMD simulations of Syk interdomain A was taken from the WT murine structure and comprised residues 115–159. As for the larger Syk construct (residues

8–261), the single phosphomimetic mutation Y130E was introduced *in silico* using PyMOL along with acetyl and N-methyl neutral caps on the N- and C-termini. Generation of all-atom topologies/parameters and the addition of solvent molecules and monovalent ions were performed as described earlier. The GROMACS MD engine (version 5.1.2; Abraham *et al.*, 2015) was used for running all simulations described in this section. Simulation parameters were similar to those described earlier, with a few exceptions. Pressure coupling was done using a Parrinello–Rahman barostat (Parrinello and Rahman, 1981), and bonds containing hydrogen atoms were constrained using the LINCS algorithm for the protein (Hess, 2008) and the SETTLE algorithm for water (Miyamoto and Kollman, 1992). A 2-fs time step was used, as hydrogen mass repartitioning was not performed for these systems.

Pilot unbiased MD runs were first run for the WT and Y130E mutant systems to determine the optimal temperature distribution. After energy minimization, a copy of each system was equilibrated at nine different temperatures equally spaced within the range 275–475 K. Energy minimization and equilibration were performed as described earlier for the unbiased simulations. Production runs (without position restraints) of 100 ns in the NVT ensemble were then performed with configurations and energies saved every 10 ps. The average energy and its SD were then computed for each of the 10 simulations for a particular system and used as input for a REMD temperature scheduler (Garcia *et al.*, 2006). This scheduler provided a temperature distribution comprising 63 temperatures within the range 275–475 K that would ensure a 20% exchange rate between all adjacent replicas in the REMD simulations. The same temperature distributions were given by this scheduler for the WT and Y130E mutant interdomain A systems.

These 63 temperatures were then used to run the REMD simulations. From the energy-minimized structures, a copy of each system was equilibrated at one of the 63 temperatures. All equilibration runs were performed as described earlier for the unbiased simulations. Production REMD runs (without position restraints) of 1.2 μ s in the NVT ensemble were then performed for each replica with configurations and energies saved every 10 ps. Alternating exchanges between adjacent replicas were attempted every 2 ps, with swap acceptance or rejection determined by the Metropolis criterion. All analyses were done using the 15 replicas with temperatures less than 310 K (excluding the 275-K replica, which acted as a sink replica). Helicity for each of the 15 replicas was monitored over the entire trajectory, while subsequent processing and analyses used the last 500 ns of these trajectories.

Hybrid MD/polymer model of multivalent interactions in WT and Y130E Syk–FceR1 γ complexes

The conformational ensembles for WT and Y130E mutant Syk interdomain A were each taken from the 15 replicas described earlier for the REMD simulations. To generate the corresponding ensembles of WT and Y130E mutant Syk tandem SH2 and interdomain A, the N-SH2 (residues 8–116) and C-SH2 (residues 158–261) from the WT murine model of Syk were reattached *in silico* to every snapshot in the interdomain A ensembles using PyMOL. In particular, the atoms in the peptide bond between residues 115 and 116 were structurally aligned between N-SH2 and each interdomain A snapshot, and similarly for the atoms in the peptide bond between residues 158 and 159 to attach C-SH2. After filtering out of snapshots containing steric clashes between N-SH2 with interdomain A, C-SH2 with interdomain A, and N-SH2 with C-SH2, around 5% of the WT snapshots remained as physically viable models of Syk tandem SH2 and interdomain A, and similarly 5% of the Y130E mutant snapshots re-

mained. The distance distribution between the two SH2 domains for each system was obtained using the distance reaction coordinate described earlier.

These inter-SH2 distance distributions were used as the MD component in the hybrid MD/polymer model to estimate the effective concentration C_{eff} in Eq. 3. The inter-ITAM-pTyr distance distribution comprised the polymer model component of this hybrid approach, and was generated using Eq. 4, which assumes that each Syk molecule binds to a single immunoreceptor tail in a *cis* mode. This equation requires a value for the peptide contour length, which represents the maximum/extended end-to-end length of the peptide as a function of the number of residues (N) (Zhou, 2001),

$$l_c = 0.38 \times N \quad (6)$$

and a value for the peptide persistence length that gives the end-to-end length of the peptide beyond which a description of its behavior transitions from a flexible rod to a random walk (Rawat and Biswas, 2009),

$$l_p = 0.074 \times N^{0.43} \quad (7)$$

A value of 12 was used for N in Eqs. 6 and 7, as this gives the length between the two pTyr residues in the FceR1 γ sequence (counting inclusive of both pTyr). C_{eff} is then calculated in Eq. 3 by integrating over the products of the probabilities in the overlapping regions between both distributions for all possible distances (Van Valen *et al.*, 2009; Sethi *et al.*, 2011). C_{eff} can then be used for estimating the equilibrium dissociation constant K_{overall}^D via Eq. 1 and getting the reciprocal.

System setup and unbiased MD simulations of WT Syk–FceR1 γ complexes with 2:2 stoichiometry

Although there are 24 possible permutations for combining four SH2 domains from two Syk molecules with four pTyrs from an FceR1 γ dimer, we found that only one *cis* and five *trans* modes can be built as physically viable structural models. The structure for the *cis* mode complex was obtained by first taking one of the Syk-CD3 ϵ structures (chains A and B) from PDB 1A81 and performing *in silico* mutagenesis with PyMOL to get the WT murine Syk and FceR1 γ sequences, and then placing two of these structures adjacent to each other. Each of the five *trans* structures was then obtained from the *cis* structure via a combination of manual translation and rotation operations in PyMOL. Backbone breaks/reseals and rotations were performed on the N-C α and C α -C bonds of the FceR1 γ chain to keep the WT structure of Syk intact and to prevent accidental formation of peptide bonds with incorrect dihedral angles (i.e., not 180°). Acetyl and N-methyl neutral caps were added to the N- and C-termini of all chains using PyMOL. Generation of all-atom topologies/parameters, addition of solvent molecules and monovalent ions, and unbiased MD simulations using GPU-optimized AMBER were performed as described earlier for the unbiased simulations of Syk tandem SH2 and interdomain A.

Reagents and antibodies

MEM was purchased from Life Technologies (Grand Island, NY). Alexa⁶⁴⁷-labeled anti-Tac IgG was purchased from BioLegend (San Diego, CA) and anti-mouse IgG was purchased from Jackson ImmunoResearch Laboratories (West Grove, PA). Amaxa Nucleofector and Solution L were purchased from Lonza (Basel, Switzerland). Fura-2AM was from Molecular Probes (Eugene, OR). DNP₂₅-BSA

was from ThermoFisher Scientific (Waltham, MA; catalogue #A23018) and anti-DNP-IgE was affinity-purified from ascites (Covance, Denver, PA) according to the methods of Liu *et al.* (1980). Alexa⁶⁴⁷-labeled IgE was prepared using Alexa⁶⁴⁷ NHS Ester (succinimidyl ester; ThermoFisher Scientific).

Cell culture and transfection

Parental RBL-2H3 cells (Metzger *et al.*, 1986; Wilson *et al.*, 2000) and their derivatives were cultured in MEM supplemented with 10% heat-inactivated fetal bovine serum, 5 U/ml penicillin, 0.05 mg/ml streptomycin, and 2 mM L-glutamine. Transient transfections were conducted using the Amaxa system (Program T-20) and cells were imaged the following day. Constructs for expression of chimeric TT- γ receptors have been described previously (Letourneur and Klausner, 1991). Constructs for reconstitution of Fc ϵ R1 γ WT and mutant γ in Fc ϵ R1 γ -KO cells were prepared in the pcDNA3.1 vector (Invitrogen). For all microscopy experiments, cells were plated overnight in eight-well Lab-Tek (Nunc) chambers (ThermoFisher Scientific) at a density of 50,000 cell/well.

Genome editing

The Fc ϵ R1 γ -KO cell line was generated in RBL-2H3 cells by CRISPR-Cas9-mediated gene editing, resulting in insertion of a premature stop codon. RNA (5'-GCAAGAACAAGATCACCGCT-3') targeting the first exon of rat Fc ϵ R1 γ was designed using the <http://crispr.mit.edu/> portal and then subcloned into PX458 vector (Addgene plasmid #48138) for simultaneous expression of gRNA, WT Cas9, and a GFP reporter. For gRNA subcloning, two partially complementary oligonucleotides (Integrated DNA Technologies) were assembled by PCR. Gel-purified PCR products were cloned into BbsI-digested PX458 using Gibson assembly (NEB) following the manufacturer's specifications. GFP-positive cells were selected on an iCyt cell sorter 24 h after transfection using the Amaxa system and then dispensed at single-cell density into 96-well plates. Subclones were screened for lack of fluorescent IgE binding by flow cytometry, followed by Western blotting to confirm selected clones completely lack Fc ϵ R1 γ expression.

Calcium measurements

Calcium measurements and data analysis were performed as previously described (Schwartz *et al.*, 2015). Parental or Fc ϵ R1 γ -KO derivatives were primed overnight with DNP-specific Alexa⁶⁴⁷-labeled IgE (1 μ g/ml). Fura-2AM loading (2 μ M in Hanks buffer) was performed for 30 min at room temperature. Cells expressing chimeric TT- γ receptors were incubated with Alexa⁶⁴⁷-labeled anti-Tac IgG (1 μ g/ml) for the final 10 min. In all cases, cells were washed with buffer and ratio images were acquired at 35°C using an Olympus IX71 inverted microscope outfitted with a UPLANSAPO 60X/NA1.2 water immersion objective coupled to an objective heater (Biopetechs). Cells were activated by cross-linking with DNP₂₅-BSA (0.1 μ g/ml; ThermoFisher Scientific catalogue #A23018) or anti-mouse IgG (25 μ g/ml), added at 30 s during a total of 5 min of imaging. Ratiometric changes in cytosolic calcium were determined by alternating between 350 and 380 nm at 1 Hz with a xenon arc lamp monochromator (Cairn Research OptoScan) and collecting the interleaved Fura-2 fluorescence emissions at 510 nm with an iXon 887 EMCCD camera using IQ3 imaging software (Andor Technology). Offline ratiometric analysis was performed over time with a custom MATLAB script for each cell (5–10 per field of view) to assess calcium release and subsequently normalized to a minimum threshold of Alexa⁶⁴⁷ emission (100 AU) based on surface expression of receptors in transiently transfected cells.

ACKNOWLEDGMENTS

This work was supported by federal grants and the New Mexico Spatiotemporal Modeling Center (NIH P50GM085273 for B.S.W.; the Department of Energy through contract DE-AC5206NA25396 for S.G. and T.T.; NIH R35GM126934 for D.S.L.). T.T. was also supported by the Center for Nonlinear Studies (CNLS) at the Los Alamos National Laboratory (LANL). E.J. was supported by K12 GM088021. Computing resources were made available through Extreme Science and Engineering Discovery Environment (XSEDE) Allocation MCB170148, which is supported by National Science Foundation (NSF) Grant ACI-1548562, and through LANL Institutional Computing. We thank Shayna Lucero for assistance with cell culture and gratefully acknowledge use of the University of New Mexico Cancer Center fluorescence microscopy and flow cytometry facilities, as well as NIH-NCI support via P30CA118100 for this core.

REFERENCES

- Abraham MJ, Murtola T, Schulz R, Páll S, Smith JC, Hess B, Lindahl E (2015). GROMACS: high performance molecular simulations through multi-level parallelism from laptops to supercomputers. *SoftwareX* 1-2, 19–25.
- Aqvist J, Medina C, Samuelsson JE (1994). A new method for predicting binding affinity in computer-aided drug design. *Protein Eng* 7, 385–391.
- Åqvist J, Wennerström P, Nervall M, Bjelic S, Brandsdal BO (2004). Molecular dynamics simulations of water and biomolecules with a Monte Carlo constant pressure algorithm. *Chem Phys Lett* 384, 288–294.
- Ardito F, Giuliani M, Perrone D, Troiano G, Lo Muzio L (2017). The crucial role of protein phosphorylation in cell signaling and its use as targeted therapy (review). *Int J Mol Med* 40, 271–280.
- Basson MA (2012). Signaling in cell differentiation and morphogenesis. *Cold Spring Harb Perspect Biol* 4, a008151.
- Bauer B, Steinle A (2017). HemITAM: a single tyrosine motif that packs a punch. *Sci Signal* 10, ean3676.
- Best RB, Zhu X, Shim J, Lopes PE, Mittal J, Feig M, Mackerell AD Jr (2012). Optimization of the additive CHARMM all-atom protein force field targeting improved sampling of the backbone ϕ , ψ and side-chain $\chi(1)$ and $\chi(2)$ dihedral angles. *J Chem Theory Comput* 8, 3257–3273.
- Blank U, Ra C, Miller L, White K, Metzger H, Kinet JP (1989). Complete structure and expression in transfected cells of high affinity IgE receptor. *Nature* 337, 187–189.
- Call ME, Schnell JR, Xu C, Lutz RA, Chou JJ, Wucherpfennig KW (2006). The structure of the $\zeta\zeta$ transmembrane dimer reveals features essential for its assembly with the T cell receptor. *Cell* 127, 355–368.
- Cambier JC (1995). Antigen and Fc receptor signaling. The awesome power of the immunoreceptor tyrosine-based activation motif (ITAM). *J Immunol* 155, 3281–3285.
- Case DA, Ben-Shalom IY, Brozell SR, Cerutti DS, Cheatham TEI, Cruzeiro VWD, Darden TA, Duke RE, Ghoreishi D, Gilson MK, *et al.* (2017). AMBER 2017, University of California, San Francisco.
- Chan AC, Iwashima M, Turck CW, Weiss A (1992). ZAP-70: a 70 kd protein-tyrosine kinase that associates with the TCR ζ chain. *Cell* 71, 649–662.
- Chen T, Repetto B, Chizzonite R, Pullar C, Burghardt C, Dharm E, Zhao Z, Carroll R, Nunes P, Basu M, *et al.* (1996). Interaction of phosphorylated Fc ϵ R1 γ immunoglobulin receptor tyrosine activation motif-based peptides with dual and single SH2 domains of p72syk. assessment of binding parameters and real time binding kinetics. *J Biol Chem* 271, 25308–25315.
- Cheng AM, Negishi I, Anderson SJ, Chan AC, Bolen J, Loh DY, Pawson T (1997). The Syk and ZAP-70 SH2-containing tyrosine kinases are implicated in pre-T cell receptor signaling. *Proc Natl Acad Sci USA* 94, 9797–9801.
- Chu DH, Morita CT, Weiss A (1998). The Syk family of protein tyrosine kinases in T-cell activation and development. *Immunol Rev* 165, 167–180.
- Cleyrat C, Girard R, Choi EH, Jeziorski É, Lavabre-Bertrand T, Hermouet S, Carillo S, Wilson BS (2017). Gene editing rescue of a novel MPL mutant associated with congenital amegakaryocytic thrombocytopenia. *Blood Adv* 1, 1815–1826.
- Darden T, York D, Pedersen L (1993). Particle mesh Ewald: an N -log(N) method for Ewald sums in large systems. *J Chem Phys* 98, 10089–10092.
- Deindl S, Kadlec TA, Brdicka T, Cao X, Weiss A, Kuriyan J (2007). Structural basis for the inhibition of tyrosine kinase activity of ZAP-70. *Cell* 129, 735–746.

- Faeder JR, Blinov ML, Goldstein B, Hlavacek WS (2005). Combinatorial complexity and dynamical restriction of network flows in signal transduction. *Syst Biol* 2, 5–15.
- Faeder JR, Hlavacek WS, Reischl I, Blinov ML, Metzger H, Redondo A, Wofsy C, Goldstein B (2003). Investigation of early events in FcεRI-mediated signaling using a detailed mathematical model. *J Immunol* 170, 3769–3781.
- Fasbender F, Claus M, Wingert S, Sandusky M, Watzl C (2017). Differential requirements for Src-family kinases in SYK or ZAP70-mediated SLP-76 phosphorylation in lymphocytes. *Front Immunol* 8, 789.
- Feenstra KA, Hess B, Berendsen HJC (1999). Improving efficiency of large time-scale molecular dynamics simulations of hydrogen-rich systems. *J Comput Chem* 20, 786–798.
- Feng C, Post CB (2016). Insights into the allosteric regulation of Syk association with receptor ITAM, a multi-state equilibrium. *Phys Chem Chem Phys* 18, 5807–5818.
- Fiebiger E, Tortorella D, Jouvin M-H, Kinet J-P, Ploegh HL (2005). Cotranslational endoplasmic reticulum assembly of FcεRI controls the formation of functional IgE-binding receptors. *J Exp Med* 201, 267–277.
- Fütterer K, Wong J, Gruzica RA, Chan AC, Waksman G (1998). Structural basis for Syk tyrosine kinase ubiquity in signal transduction pathways revealed by the crystal structure of its regulatory SH2 domains bound to a dually phosphorylated ITAM peptide. *J Mol Biol* 281, 523–537.
- Garcia AE, Herce H, Paschek D (2006). Simulations of temperature and pressure unfolding of peptides and proteins with replica exchange molecular dynamics. *Annu Rep Comput Chem* 2, 83–95.
- Garcia AE, Sanbonmatsu KY (2001). Exploring the energy landscape of a beta hairpin in explicit solvent. *Proteins* 42, 345–354.
- Geahlen RL (2009). Syk and pTyr^d: signaling through the B cell antigen receptor. *Biochim Biophys Acta* 1793, 1115–1127.
- Geahlen RL, Burg DL (1994). The role of Syk in cell signaling. *Adv Exp Med Biol* 365, 103–109.
- Gelens L, Qian J, Bollen M, Saurin AT (2018). The importance of kinase-phosphatase integration: lessons from mitosis. *Trends Cell Biol* 28, 6–21.
- Getahun A, Beavers NA, Larson SR, Shlomchik MJ, Cambier JC (2016). Continuous inhibitory signaling by both SHP-1 and SHIP-1 pathways is required to maintain unresponsiveness of anergic B cells. *J Exp Med* 213, 751–769.
- Graus MS, Wester MJ, Lowman DW, Williams DL, Kruppa MD, Martinez CM, Young JM, Pappas HC, Lidke KA, Neumann AK (2018). Mannan molecular substructures control nanoscale glucan exposure in *Candida*. *Cell Rep* 24, 2432–2442.
- Harris LJ, Skaletsky E, McPherson A (1998). Crystallographic structure of an intact IgG1 monoclonal antibody. *J Mol Biol* 275, 861–872.
- Harwood NE, Batista FD (2008). New insights into the early molecular events underlying B cell activation. *Immunity* 28, 609–619.
- Hatada MH, Lu X, Laird ER, Green J, Morgenstern JP, Lou M, Marr CS, Phillips TB, Ram MK, Theriault K, et al. (1995). Molecular basis for interaction of the protein tyrosine kinase ZAP-70 with the T-cell receptor. *Nature* 377, 32–38.
- Hess B (2008). P-LINCS: a parallel linear constraint solver for molecular simulation. *J Chem Theory Comput* 4, 116–122.
- Hughes CE, Pollitt AY, Mori J, Eble JA, Tomlinson MG, Hartwig JH, Callaghan CA, Fütterer K, Watson SP (2010). CLEC-2 activates Syk through dimerization. *Blood* 115, 2947–2955.
- Hunter T (1995). Protein kinases and phosphatases: the yin and yang of protein phosphorylation and signaling. *Cell* 80, 225–236.
- Iwashima M, Irving BA, van Oers NS, Chan AC, Weiss A (1994). Sequential interactions of the TCR with two distinct cytoplasmic tyrosine kinases. *Science* 263, 1136–1139.
- Ji QS, Chattopadhyay A, Vecchi M, Carpenter G (1999). Physiological requirement for both SH2 domains for phospholipase C-γ1 function and interaction with platelet-derived growth factor receptors. *Mol Cell Biol* 19, 4961–4970.
- Jiang K, Zhong B, Ritchey C, Gilvary DL, Hong-Geller E, Wei S, Djeu JY (2003). Regulation of Akt-dependent cell survival by Syk and Rac. *Blood* 101, 236–244.
- Johnson SA, Pleiman CM, Pao L, Schneringer J, Hippen K, Cambier JC (1995). Phosphorylated immunoreceptor signaling motifs (ITAMs) exhibit unique abilities to bind and activate Lyn and Syk tyrosine kinases. *J Immunol* 155, 4596–4603.
- Jorgensen WL, Chandrasekhar J, Madura JD, Impey RW, Klein ML (1983). Comparison of simple potential functions for simulating liquid water. *J Chem Phys* 79, 926–935.
- Kawakami Y, Kitaura J, Hartman SE, Lowell CA, Siraganian RP, Kawakami T (2000). Regulation of protein kinase Cβ1 by two protein-tyrosine kinases, Btk and Syk. *Proc Natl Acad Sci USA* 97, 7423–7428.
- Keshvara LM, Isaacson C, Harrison ML, Geahlen RL (1997). Syk activation and dissociation from the B-cell antigen receptor is mediated by phosphorylation of tyrosine 130. *J Biol Chem* 272, 10377–10381.
- Keshvara LM, Isaacson CC, Yankee TM, Sarac R, Harrison ML, Geahlen RL (1998). Syk- and Lyn-dependent phosphorylation of Syk on multiple tyrosines following B cell activation includes a site that negatively regulates signaling. *J Immunol* 161, 5276–5283.
- Kihara H, Siraganian RP (1994). Src homology 2 domains of Syk and Lyn bind to tyrosine-phosphorylated subunits of the high affinity IgE receptor. *J Biol Chem* 269, 22427–22432.
- Klauda JB, Venable RM, Freites JA, O'Connor JW, Tobias DJ, Mondragon-Ramirez C, Vorobyov I, MacKerell AD Jr, Pastor RW (2010). Update of the CHARMM all-atom additive force field for lipids: validation on six lipid types. *J Phys Chem B* 114, 7830–7843.
- Kong GH, Bu JY, Kurosaki T, Shaw AS, Chan AC (1995). Reconstitution of Syk function by the ZAP-70 protein tyrosine kinase. *Immunity* 2, 485–492.
- Kuriyan J, Cowburn D (1993). Structures of SH2 and SH3 domains. *Curr Opin Struct Biol* 3, 828–837.
- Ladbury JE, Lemmon MA, Zhou M, Green J, Botfield MC, Schlessinger J (1995). Measurement of the binding of tyrosyl phosphopeptides to SH2 domains: a reappraisal. *Proc Natl Acad Sci USA* 92, 3199–3203.
- Letourneur F, Klausner RD (1991). T-cell and basophil activation through the cytoplasmic tail of T-cell-receptor zeta family proteins. *Proc Natl Acad Sci USA* 88, 8905–8909.
- Liu FT, Bohn JW, Ferry EL, Yamamoto H, Molinaro CA, Sherman LA, Klinman NR, Katz DH (1980). Monoclonal dinitrophenyl-specific murine IgE antibody: preparation, isolation, and characterization. *J Immunol* 124, 2728–2737.
- Lopez CA, Sethi A, Goldstein B, Wilson BS, Gnanakaran S (2015). Membrane-mediated regulation of the intrinsically disordered CD3 cytoplasmic tail of the TCR. *Biophys J* 108, 2481–2491.
- MacGlashan D Jr (2008). IgE receptor and signal transduction in mast cells and basophils. *Curr Opin Immunol* 20, 717–723.
- Mahajan A, Barua D, Cutler P, Lidke DS, Espinoza FA, Pehlke C, Grattan R, Kawakami Y, Tung C-S, Bradbury ARM, et al. (2014). Optimal aggregation of FcεRI with a structurally defined trivalent ligand overrides negative regulation driven by phosphatases. *ACS Chem Biol* 9, 1508–1519.
- Metzger H, Alcaraz G, Hohman R, Kinet JP, Pribluda V, Quarto R (1986). The receptor with high affinity for immunoglobulin E. *Annu Rev Immunol* 4, 419–470.
- Miyamoto S, Kollman PA (1992). Settle: an analytical version of the SHAKE and RATTLE algorithm for rigid water models. *J Comput Chem* 13, 952–962.
- Mocsai A, Ruland J, Tybulewicz VL (2010). The SYK tyrosine kinase: a crucial player in diverse biological functions. *Nat Rev Immunol* 10, 387–402.
- Molfetta R, Peruzzi G, Santoni A, Paolini R (2007). Negative signals from FcεRI engagement attenuate mast cell functions. *Arch Immunol Ther Exp* 55, 219–229.
- Mukai K, Tsai M, Saito H, Galli SJ (2018). Mast cells as sources of cytokines, chemokines, and growth factors. *Immunol Rev* 282, 121–150.
- Nimmerjahn F, Ravetch JV (2008). Fcγ receptors as regulators of immune responses. *Nat Rev Immunol* 8, 34–47.
- Ohashi T, Galiacy SD, Briscoe G, Erickson HP (2007). An experimental study of GFP-based FRET, with application to intrinsically unstructured proteins. *Protein Sci* 16, 1429–1438.
- O'Neill SK, Getahun A, Gauld SB, Merrell KT, Tamir I, Smith MJ, Dal Porto JM, Li QZ, Cambier JC (2011). Monophosphorylation of CD79a and CD79b ITAM motifs initiates a SHIP-1 phosphatase-mediated inhibitory signaling cascade required for B cell anergy. *Immunity* 35, 746–756.
- Ottinger EA, Botfield MC, Shoelson SE (1998). Tandem SH2 domains confer high specificity in tyrosine kinase signaling. *J Biol Chem* 273, 729–735.
- Panayotou G, Gish G, End P, Truong O, Gout I, Dhand R, Fry MJ, Hiles I, Pawson T, Waterfield MD (1993). Interactions between SH2 domains and tyrosine-phosphorylated platelet-derived growth factor β-receptor sequences: analysis of kinetic parameters by a novel biosensor-based approach. *Mol Cell Biol* 13, 3567–3576.
- Parrinello M, Rahman A (1981). Polymorphic transitions in single crystals: a new molecular dynamics method. *J Appl Phys* 52, 7182–7190.
- Pastor RW, Brooks BR, Szabo A (1988). An analysis of the accuracy of Langevin and molecular dynamics algorithms. *Mol Phys* 65, 1409–1419.
- Pawson T (1995). Protein modules and signalling networks. *Nature* 373, 573–580.
- Pawson T, Scott JD (2005). Protein phosphorylation in signaling—50 years and counting. *Trends Biochem Sci* 30, 286–290.

- Pei D, Wang J, Walsh CT (1996). Differential functions of the two Src homology 2 domains in protein tyrosine phosphatase SH-PTP1. *Proc Natl Acad Sci USA* 93, 1141–1145.
- Pluskey S, Wandless TJ, Walsh CT, Shoelson SE (1995). Potent stimulation of SH-PTP2 phosphatase activity by simultaneous occupancy of both SH2 domains. *J Biol Chem* 270, 2897–2900.
- Ra C, Jouvin MH, Kinet JP (1989). Complete structure of the mouse mast cell receptor for IgE (FcεRI) and surface expression of chimeric receptors (rat–mouse–human) on transfected cells. *J Biol Chem* 264, 15323–15327.
- Rawat N, Biswas P (2009). Size, shape, and flexibility of proteins and DNA. *J Chem Phys* 131, 165104.
- Reth M (1989). Antigen receptor tail clue. *Nature* 338, 383–384.
- Reth M (2001). Oligomeric antigen receptors: a new view on signaling for the selection of lymphocytes. *Trends Immunol* 22, 356–360.
- Richardson CD, Ray GJ, DeWitt MA, Curie GL, Corn JE (2016). Enhancing homology-directed genome editing by catalytically active and inactive CRISPR-Cas9 using asymmetric donor DNA. *Nat Biotechnol* 34, 339–344.
- Rivera J, Fierro NA, Olivera A, Suzuki R (2008). New insights on mast cell activation via the high affinity receptor for IgE. *Adv Immunol* 98, 85–120.
- Roy A, Hua DP, Post CB (2016). Analysis of multidomain protein dynamics. *J Chem Theory Comput* 12, 274–280.
- Ryckaert J-P, Ciccotti G, Berendsen HJC (1977). Numerical integration of the cartesian equations of motion of a system with constraints: molecular dynamics of n-alkanes. *J Comput Phys* 23, 327–341.
- Salomon-Ferrer R, Case DA, Walker RC (2012). An overview of the Amber biomolecular simulation package. *WIREs Comput Mol Sci* 3, 198–210.
- Schwartz SL, Cleyrat C, Olah MJ, Relich PK, Phillips GK, Hlavacek WS, Lidke KA, Wilson BS, Lidke DS (2017). Differential mast cell outcomes are sensitive to FcεRI–Syk binding kinetics. *Mol Biol Cell* 28, 3397–3414.
- Schwartz SL, Yan Q, Telmer CA, Lidke KA, Bruchez MP, Lidke DS (2015). Fluorogen-activating proteins provide tunable labeling densities for tracking FcεRI independent of IgE. *ACS Chem Biol* 10, 539–546.
- Sethi A, Goldstein B, Gnanakaran S (2011). Quantifying intramolecular binding in multivalent interactions: a structure-based synergistic study on Grb2–Sos1 complex. *PLoS Comput Biol* 7, e1002192.
- Shiue L, Zoller MJ, Brugge JS (1995). Syk is activated by phosphotyrosine-containing peptides representing the tyrosine-based activation motifs of the high affinity receptor for IgE. *J Biol Chem* 270, 10498–10502.
- Sigalov A (2005). Multi-chain immune recognition receptors: spatial organization and signal transduction. *Semin Immunol* 17, 51–64.
- Siraganian RP (2003). Mast cell signal transduction from the high-affinity IgE receptor. *Curr Opin Immunol* 15, 639–646.
- Smith AJ, Surviladze Z, Gaudet EA, Backer JM, Mitchell CA, Wilson BS (2001). p110β and p110δ phosphatidylinositol 3-kinases up-regulate FcεRI-activated Ca²⁺ influx by enhancing inositol 1,4,5-trisphosphate production. *J Biol Chem* 276, 17213–17220.
- Smith-Garvin JE, Koretzky GA, Jordan MS (2009). T cell activation. *Annu Rev Immunol* 27, 591–619.
- Songyang Z, Shoelson SE, Chaudhuri M, Gish G, Pawson T, Haser WG, King F, Roberts T, Ratnofsky S, Lechleider RJ, et al. (1993). SH2 domains recognize specific phosphopeptide sequences. *Cell* 72, 767–778.
- Sugita Y, Okamoto Y (1999). Replica-exchange molecular dynamics method for protein folding. *Chem Phys Lett* 314, 141–151.
- Tamir I, Cambier JC (1998). Antigen receptor signaling: integration of protein tyrosine kinase functions. *Oncogene* 17, 1353–1364.
- Turner H, Kinet JP (1999). Signalling through the high-affinity IgE receptor FcεRI. *Nature* 402, 24–30.
- Van den Herik-Oudijk IE, Capel PJ, van der Bruggen T, Van de Winkel JG (1995). Identification of signaling motifs within human Fc gamma RIIa and Fc gamma RIIb isoforms. *Blood* 85, 2202–2211.
- Van Valen D, Haataja M, Phillips R (2009). Biochemistry on a leash: the roles of tether length and geometry in signal integration proteins. *Biophys J* 96, 1275–1292.
- Wan Y, Kurosaki T, Huang XY (1996). Tyrosine kinases in activation of the MAP kinase cascade by G-protein-coupled receptors. *Nature* 380, 541–544.
- Wang H, Kadlecsek TA, Au-Yeung BB, Goodfellow HE, Hsu LY, Freedman TS, Weiss A (2010). ZAP-70: an essential kinase in T-cell signaling. *Cold Spring Harb Perspect Biol* 2, a002279.
- Wester MJ, Lin J, Neumann AK (2017). A computational model for regulation of nanoscale glucan exposure in *Candida albicans*. *PLoS One* 12, e0188599.
- Wilson BS, Kapp N, Lee RJ, Pfeiffer JR, Martinez AM, Platt Y, Letourneur F, Oliver JM (1995). Distinct functions of the FcεR1 γ and β subunits in the control of FcεR1-mediated tyrosine kinase activation and signaling responses in RBL-2H3 mast cells. *J Biol Chem* 270, 4013–4022.
- Wilson BS, Pfeiffer JR, Oliver JM (2000). Observing FcεRI signaling from the inside of the mast cell membrane. *J Cell Biol* 149, 1131–1142.
- Yamashita T, Suzuki R, Backlund PS, Yamashita Y, Yergey AL, Rivera J (2008). Differential dephosphorylation of the FcγR immunoreceptor tyrosine-based activation motif tyrosines with dissimilar potential for activating Syk. *J Biol Chem* 283, 28584–28594.
- Yan Q, Barros T, Visperas PR, Deindl S, Kadlecsek TA, Weiss A, Kuriyan J (2013). Structural basis for activation of ZAP-70 by phosphorylation of the SH2-kinase linker. *Mol Cell Biol* 33, 2188–2201.
- Zhang Y, Oh H, Burton RA, Burgner JW, Geahlen RL, Post CB (2008). Tyr130 phosphorylation triggers Syk release from antigen receptor by long-distance conformational uncoupling. *Proc Natl Acad Sci USA* 105, 11760–11765.
- Zhou H-X (2001). Loops in proteins can be modeled as worm-like chains. *J Phys Chem B* 105, 6763–6766.